Chemical Science

ROYAL SOCIETY OF CHEMISTRY

REVIEW

View Article Online
View Journal | View Issue

Check for updates

Cite this: *Chem. Sci.*, 2026, **17**, 3958

Mechanism-guided design of specific-activated photosensitizers for precision photodynamic therapy

Kai Wang,[a] Xiaoying Mao,[a] Wuyan Xie,[a] Xiaoyan Liu,[a] Qin Zhou,[a] Dan Wu,[b] Qing Zhu *[a] and Bin Liu *[c]

Received 4th December 2025
Accepted 28th January 2026

DOI: 10.1039/d5sc09499b

rsc.li/chemical-science

The clinical application of conventional photodynamic therapy (PDT) is often limited by the nonspecific phototoxicity of "always-on" photosensitizers. Activatable photosensitizers (aPSs) have emerged as a promising solution to this challenge. These smart agents are designed to remain inactive under normal physiological conditions and become activated only by disease-specific stimuli, thereby significantly improving treatment specificity and safety. This review summarizes the key design strategies for developing effective aPSs. We focus on the general principles of utilizing various quenching mechanisms, such as energy or electron transfer processes and aggregation behavior control, to suppress photosensitizer activity until a specific trigger is encountered. Representative examples are discussed to illustrate how these designs respond to biomarkers like enzymes, glutathione, or acidic pH to activate therapeutic functions. By minimizing off-target effects and enhancing spatial control, these mechanism-guided approaches pave the way for more precise and clinically viable PDT protocols, aligning with the core objectives of precision medicine.

Open Access Article. Published on 29 January 2026. Downloaded on 5/27/2026 1:04:59 AM.
This article is licensed under a Creative Commons Attribution-NonCommercial 3.0 Unported Licence.

1 Introduction

Since Raab and von Tappeiner first reported the light-induced cytotoxicity of certain dyes in the early 20th century, PDT has evolved for more than a century.[1,2] As a treatment combining photosensitizers (PSs), light, and O_2, PDT offers clear advantages over traditional chemotherapy and radiotherapy.[3] Its spatiotemporal controllability allows accurate adjustment of the light position, dose, and duration, enabling localized tumor treatment while reducing systemic toxicity.[4,5] Beyond directly causing apoptosis or necrosis through generation of reactive oxygen species (ROS), PDT can also trigger immunogenic cell death (ICD), which activates antitumor immune responses and creates a synergistic link between local tumor damage and immune regulation.[6,7] PDT can further inhibit tumor angiogenesis and remodel the tumor microenvironment (TME), and it can be repeatedly applied with minimal risk of drug resistance.[8–13] In recent years, several PSs, such as Photofrin, Verteporfin, Tookad, and Akalux have been approved for clinical use in treating cancers of the skin, lung, esophagus, and bladder and age-related macular degeneration.[14,15] With high selectivity and multiple therapeutic pathways, PDT is becoming a promising option for precise and minimally invasive cancer treatment.[16–18]

The effectiveness of PDT depends on the efficient activation of PSs under light irradiation. After absorbing light of a specific wavelength, the PS is excited from the ground singlet state S_0 to a short-lived high-energy singlet state S_n and then quickly relaxes to the lowest excited singlet state S_1 through internal conversion. From S_1, the PS can deactivate through two main routes: some molecules return to the ground state by fluorescence emission, while others undergo intersystem crossing to form a long-lived triplet state T_1. The triplet PS serves as the key intermediate in PDT and generates ROS through two photochemical pathways, known as Type I and Type II reactions (Fig. 1). In the Type I pathway, the excited PS reacts with nearby biomolecules such as lipids, proteins, or nucleic acids through electron or hydrogen transfer, producing radical intermediates like $PS^{\bullet-}$ or $PS^{\bullet+}$. These radicals then react with O_2 to form superoxide anions $O_2^{\bullet-}$, which can further produce H_2O_2 or hydroxyl radicals $^{\bullet}OH$. This pathway strongly depends on the redox potential of the PS and the surrounding microenvironment, including the oxygen level, pH, and substrate availability.[19–21] In the Type II pathway, the triplet PS transfers energy directly to ground-state triplet oxygen ($^3O_2$) to form singlet oxygen ($^1O_2$), which is considered the main reactive species responsible for PDT-induced cellular damage.[22,23]

[a]*College of Biotechnology and Bioengineering, Zhejiang University of Technology, Chaowang Road 18, Hangzhou 310014, China. E-mail: zhuq@zjut.edu.cn*

[b]*College of Materials Science and Engineering, Zhejiang University of Technology, Chaowang Road 18, Hangzhou 310014, China*

[c]*Department of Chemical and Biomolecular Engineering, National University of Singapore, 4 Engineering Drive 4, Singapore 117583, Singapore. E-mail: cheliub@nus.edu.sg*

© 2026 The Author(s). Published by the Royal Society of Chemistry

Open Access Article. Published on 29 January 2026. Downloaded on 5/27/2026 1:04:59 AM. This article is licensed under a Creative Commons Attribution-NonCommercial 3.0 Unported Licence.

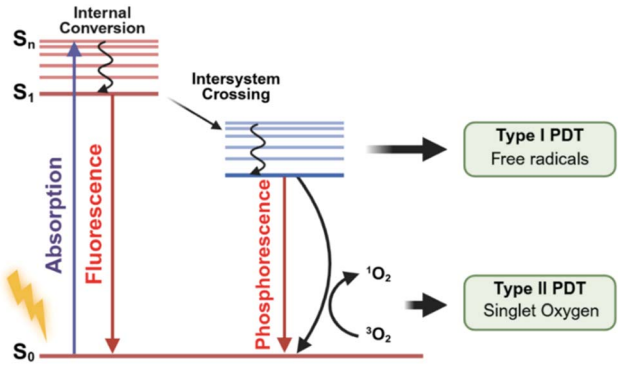

Fig. 1 Electronic transitions of photosensitizers that generate ROS during PDT.

The photochemical efficiency of PSs is crucial for effective PDT, but their strong ability to generate ROS also poses the risk of unwanted phototoxicity.[24–26] When too many ROS are produced, they can damage normal tissues within the illuminated area, leading to inflammation, vascular injury, or unintended cell death.[27] Local delivery methods, such as intratumoral injection, can help reduce systemic or skin toxicity, but they cannot fully stop light-exposed healthy tissues from being affected.[28] Clinical findings have confirmed these safety concerns, as serious cardiopulmonary problems and local tissue injuries have been observed in patients treated with Photofrin® or Visudyne®-based PDT.[29–31] These cases show the difficulty of achieving complete spatial selectivity *in vivo*.

To enhance the precision of PDT, two main strategies have been developed: molecular targeting and activation-based control.[32,33] Targeted PSs can improve accumulation in diseased tissue through ligand recognition, but they still face the problem of off-target activation when exposed to light, which may cause unintended tissue damage.[34,35] In contrast, aPSs represent a new class of PDT agents that stay non-reactive during circulation and become active only in response to specific biological signals such as abnormal pH, redox imbalance, or high enzyme activity.[36] This activation-based mechanism limits PDT effects to diseased regions in both space and time, greatly reducing harm to normal tissues. Clinically, aPSs show strong potential to solve one of the major problems of traditional and targeted PDT, nonspecific phototoxicity, by combining sensitive diagnosis with controllable treatment.[37,38] With rational molecular or supramolecular design, aPSs provide a promising path toward safer, more selective, and personalized PDT in line with the goals of precision medicine.[39]

The realization of precise activation in aPSs fundamentally relies on rational molecular design. Whether a PS can stay optically silent under physiological conditions and then be efficiently activated by disease-specific cues is determined by its photophysical properties and electronic regulation. Over the past decade, various molecular engineering strategies have been developed to control intramolecular energy or electron transfer pathways, including intramolecular charge transfer (ICT), photoinduced electron transfer (PET), Förster resonance energy transfer (FRET), aggregation-induced emission (AIE), aggregation-caused quenching (ACQ), and tetrazine-mediated quenching systems.[40,41] Each mechanism offers a distinct way to modulate fluorescence and ROS generation of PSs, allowing precise control over their optical and photodynamic outputs. Beyond simply switching luminescence on or off, these strategies allow aPSs to incorporate multiple responsiveness elements such as enzymatic activity, pH changes, redox imbalance, or hypoxia, creating a direct link between photophysical behavior and pathological microenvironments. Integrating these mechanisms not only improves therapeutic selectivity and reduces off-target phototoxicity but also enables real-time diagnostic imaging and treatment monitoring.

The seminal review by Li *et al.* offered a pioneering summary of aPSs, effectively transitioning the field from conventional dyes to "smart", stimuli-responsive theranostics. By systematically categorizing diverse triggers—including tumor acidity, elevated glutathione levels, and enzymatic activity—their work established a framework for achieving precise spatiotemporal control over singlet oxygen generation.[42] In recent years, several reviews have summarized aPSs from different perspectives such as biological targets, activation triggers, or structural families.[43–47] Despite these efforts, one essential dimension remains insufficiently addressed: the classification of aPSs based on their quenching mechanisms. These mechanisms, including pathways that regulate excited-state energy dissipation or suppress ROS generation, are the fundamental determinants of whether a PS can remain optically silent in physiological environments and be selectively activated within disease sites. This mechanistic viewpoint is of particular significance because quenching processes directly shape crucial parameters such as off-state leakage, activation contrast, ROS output efficiency, photostability, and the overall fidelity of spatiotemporal control. A precise understanding of how quenching governs the on/off photophysical transitions is therefore central to the rational engineering of aPSs with predictable and tunable activation behaviors. Yet the current literature seldom organizes aPSs within a unified framework grounded in these photophysical suppression pathways.

To fill this gap, the present review systematically categorizes aPSs according to their underlying quenching mechanisms, establishing a mechanism-centered framework that links excited-state regulation with activation performance. By consolidating diverse molecular designs under this photophysical logic, this review clarifies the fundamental activation pathways, distills cross-platform design principles, and provides a coherent conceptual foundation for developing next-generation aPSs with higher selectivity, stronger signal-to-background ratios, and improved therapeutic reliability.

In the following sections, representative activation mechanisms of aPSs will be summarized, with a focus on the molecular design logic, activation principles, and structure–function relationships. Understanding these mechanisms provides a blueprint for developing next generation aPSs with higher precision, deeper tissue penetration, and better clinical translatability in PDT.

Open Access Article. Published on 29 January 2026. Downloaded on 5/27/2026 1:04:59 AM. This article is licensed under a Creative Commons Attribution-NonCommercial 3.0 Unported Licence.

2 FRET-based design of aPSs

2.1 Design principles and basic mechanisms

FRET represents one of the most fundamental strategies for constructing aPSs.[48] In a typical FRET-based design, an excited PS transfers its excitation energy non-radiatively to a nearby quencher, effectively suppressing intersystem crossing and consequently inhibiting ROS generation.[49] The efficiency of this process is primarily determined by three photophysical parameters: the degree of spectral overlap between donor emission and acceptor absorption, the donor–acceptor distance which usually falls within the 10–100 Å range where dipole–dipole coupling remains effective, and the relative orientation of the transition dipoles that dictates the strength and directionality of energy transfer. To ensure robust quenching, donor and acceptor units are often connected through carefully engineered spacers such as flexible alkyl chains, short peptide sequences, or nucleic acid fragments. These structural elements allow fine control over molecular distance, mobility, and geometric arrangement, which are all essential for maintaining an optimal FRET configuration. In addition, the local microenvironment surrounding the aPS, including solvent polarity, viscosity, and the degree of molecular restriction, can further influence conformational dynamics and dipole alignment, thereby modulating overall FRET efficiency.[50,51]

Conceptually, a FRET-based aPS can be viewed as a molecular dyad composed of a PS and a responsive quencher linked by a cleavable or conformation-dependent bridge. The activation process involves disruption of the energy transfer pathway through structural or chemical changes within this linkage, resulting in recovery of fluorescence and photosensitizing activity (Fig. 2A). For example, Wang *et al.* reported an azo-PDT system in which an azo linker connects the PS Pyro with the Near-Infrared (NIR) fluorophore SiR-665.[52] The design uses an FRET effect to suppress both fluorescence and phototoxicity under normoxic conditions. In hypoxic tumor environments, the azo bond undergoes reductive cleavage, which removes this suppression and enables tumor-specific fluorescence imaging and PDT (Fig. 2B). Such a modular design framework provides a versatile foundation for tailoring aPSs with desired switching behaviors and activation mechanisms (Table 1 and Fig. 4).

2.2 Recent progress in FRET-based aPSs

In FRET-based aPSs, controlling the proximity between the donor and acceptor is the key factor determining energy transfer efficiency. Careful design of the chemical linkage between the PS and quencher dictates whether the system stays in an off or on photodynamic state. Among biological stimuli, glutathione (GSH), which is present at much higher levels in the tumor cytoplasm than in normal tissues, provides an ideal internal trigger for selective activation.[45,46] To take advantage of this redox gradient, FRET systems often use disulfide bonds as dynamic linkers.[64] These bonds can be cleaved by intracellular GSH, causing the donor and acceptor to separate and restoring fluorescence and ROS production. This simple but effective strategy allows precise control of the FRET process and has been widely used in designing GSH-responsive aPS for tumor-selective PDT.

Building on this strategy, Shi *et al.* reported in 2019 an intelligent FRET-based aPS composed of zinc phthalocyanine (ZnPc) as the ROS-generating donor and a ferrocenyl-substituted BODIPY as a NIR dark quencher.[56] The donor and acceptor were connected through a GSH-cleavable disulfide bond, allowing simultaneous control of FRET and PET processes. When exposed to intracellular GSH (2–4 mM, 37 °C), the disulfide bond was cleaved, separating the quencher and markedly enhancing fluorescence (~8-fold at 704 nm) and singlet oxygen generation (up to 5-fold). A non-cleavable analogue showed negligible change. In HT29 cells, the cleavable aPS displayed 1.6-fold higher intracellular fluorescence than the non-cleavable version and a significantly lower IC_{50} under irradiation (0.42 μM *vs.* 1.42 μM), confirming effective GSH-triggered activation and phototoxicity. *In vivo* imaging further revealed sustained tumor fluorescence up to 48 h after intratumoral injection, while the non-cleavable control produced

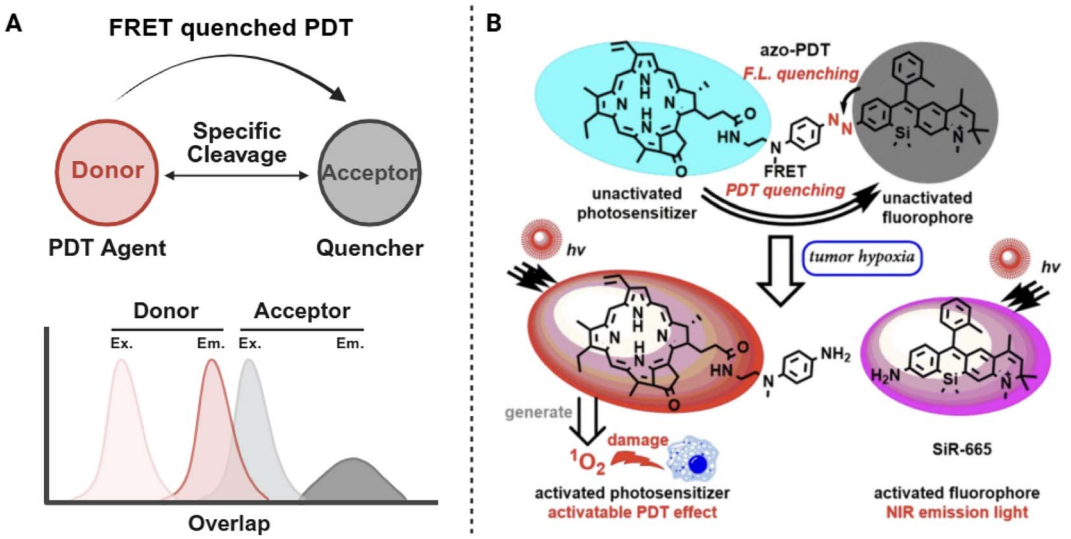

Fig. 2 Basic principle (A) and example (B) of FRET based aPS design. Reproduced with permission from ref. 52. Copyright 2020, Springer Nature.

© 2026 The Author(s). Published by the Royal Society of Chemistry

Open Access Article. Published on 29 January 2026. Downloaded on 5/27/2026 1:04:59 AM. This article is licensed under a Creative Commons Attribution-NonCommercial 3.0 Unported Licence.

Table 1 FRET based aPS design

Response factors	Range of stimulation	Response moiety	Photosensitizer	Fluorescence activation	ROS activation	Ref.
MMP-7	>8 nM	Peptide	PPa	×12	×18	53
MMP-9	>6 nM	Peptide	PPa	—	—	54
GSH	—	Disulfide bond	PPa	×149	×100+	55
GSH	0–4 mM	Disulfide bond	ZnPc	×8	×4	56
CTSB	—	Peptide	ZnPc	—	—	57
GSH/pH	∼1.0 mM	Aryl chloride	BODIPY	—	×10	58
GSH	∼10 mM	Disulfide bond	BODIPY	×∼4	—	59
HClO	0–100 μM	Thioether	TPA	×22	—	60
Hypoxia	—	Azobenzene	PPa	×∼15	×∼20	52
pH	pH 5.5–7.4	Hydrazone	ZnPc	×∼2	×∼2	61
CTSB/MMP-2	2 μg per mL (MMP-2) 1 U per mL (cathepsin B)	Peptide	DSBDP	—	—	62
GSH	0–10 mM	F_4TCNQ	TPA	—	—	63

a minimal signal. This work highlighted ferrocenyl-BODIPY as an efficient and tunable dark quencher and established disulfide-mediated FRET as a powerful approach for designing GSH-responsive aPSs for tumor-selective imaging and PDT.

Similarly, Cao *et al.* reported a GSH-activatable aPS using a FRET-quenching design (Fig. 3A). This system employed two BODIPY derivatives as the PS and quencher, linked through a GSH-cleavable disulfide bond.[59] In its intact form, efficient FRET kept the PS off by suppressing fluorescence and singlet oxygen generation. In a GSH-rich TME, disulfide cleavage disrupted FRET, restoring photoreactivity and fluorescence. Spectroscopic studies showed that 8a remained stable in 2 μM GSH, while in 10 mM GSH about 77% of the conjugate was activated within 720 min following pseudo-first-order kinetics ($k_{obs} = 5.8 \times 10^{-3}$ min^{-1}). In cancer cells including A549, HeLa, and H22, the system displayed strong GSH-dependent fluorescence recovery and ROS production, with IC_{50} values below 0.7 μM, whereas low-GSH fibroblasts showed negligible responses. *In vivo*, the PS selectively accumulated in tumors and was efficiently activated, resulting in significant tumor growth inhibition under 670 nm irradiation without systemic toxicity.

In small-molecule PS systems, GSH can trigger a switch from off to on by cleaving chemical bonds, which has been well demonstrated; meanwhile, nanomaterial-based platforms have also shown immense potential in tumor therapy by providing a modular architecture to integrate targeted delivery with programmable, deep-tissue penetration for the treatment of deep-seated tumors.[65–68] In more complex tumor environments, incorporating a GSH-responsive mechanism into a nanodelivery system can further improve PS stability *in vivo* and extend circulation time. It also allows integration with targeting and multimodal therapy functions, enabling more precise tumor treatment. Nanomaterials offer advantages such as modifiability, tumor accumulation through the enhanced permeability and retention (EPR) effect, and the ability to combine PSs with immune modulators, making them an important direction for GSH-responsive aPS research. Based on this concept, researchers developed a redox-activated porphyrin-based liposome system (RAL) to combine PDT and immunotherapy[55] (Fig. 3B). The system is formed by self-assembly of porphyrin–lipid conjugates into liposomes and uses remote loading to encapsulate the indoleamine 2,3-dioxygenase (IDO) inhibitor NLG-8189, creating IND@RAL nanoparticles. Under normal physiological conditions, homotransfer fluorescence resonance energy transfer (HOMO-FRET) between porphyrin units keeps fluorescence and PDT activity off. In tumor cells, high GSH cleaves the disulfide bonds in the liposomes, triggering an exponential increase in fluorescence and PDT activity (>100-fold) and releasing the encapsulated drug. After activation, IND@RAL under 660 nm laser irradiation efficiently generates ROS, disrupting mitochondrial membrane potential and inducing ICD, as indicated by calreticulin exposure, high mobility group box 1 (HMGB1) release, and adenosine triphosphate (ATP) secretion. The released IDO inhibitor blocks the Trp-Kyn pathway, reverses the immunosuppressive TME, and promotes $CD8^+$ T cell infiltration. In a 4T1 breast cancer model, IND@RAL showed prolonged circulation time (half-life extended from 1.17 h to 8.23 h) and tumor accumulation more than 11 times higher than that for the free drug. This treatment effectively inhibited primary tumor growth, suppressed distant metastases, and significantly improved survival without obvious toxicity to major organs. To further enhance specificity and overcome the limitations of ACQ, Teng *et al.* developed a "dual lock-and-key" supramolecular photosensitizer, BIBCl-PAE NPs. This system integrates pH-responsive micelle disassembly with a GSH-triggered aromatic nucleophilic substitution that initiates the FRET process. This dual-stimulus logic ensures that photoreactivity is exclusively restored within the acidic and GSH-rich TME, achieving a 10-fold increase in singlet oxygen generation compared to the inactive state. Such multifaceted control provides a more robust strategy for minimizing off-target phototoxicity in complex biological environments.[58]

The GSH-triggered cleavage of disulfide bonds effectively controls donor–acceptor interactions within PSs, providing high tumor specificity while keeping activity low in normal tissues. Building on this concept of regulating molecular donor–acceptor relationships, enzyme-responsive systems offer another important approach. In these systems, disease-specific proteases selectively unlock PS activity, providing

Open Access Article. Published on 29 January 2026. Downloaded on 5/27/2026 1:04:59 AM.
This article is licensed under a Creative Commons Attribution-NonCommercial 3.0 Unported Licence.

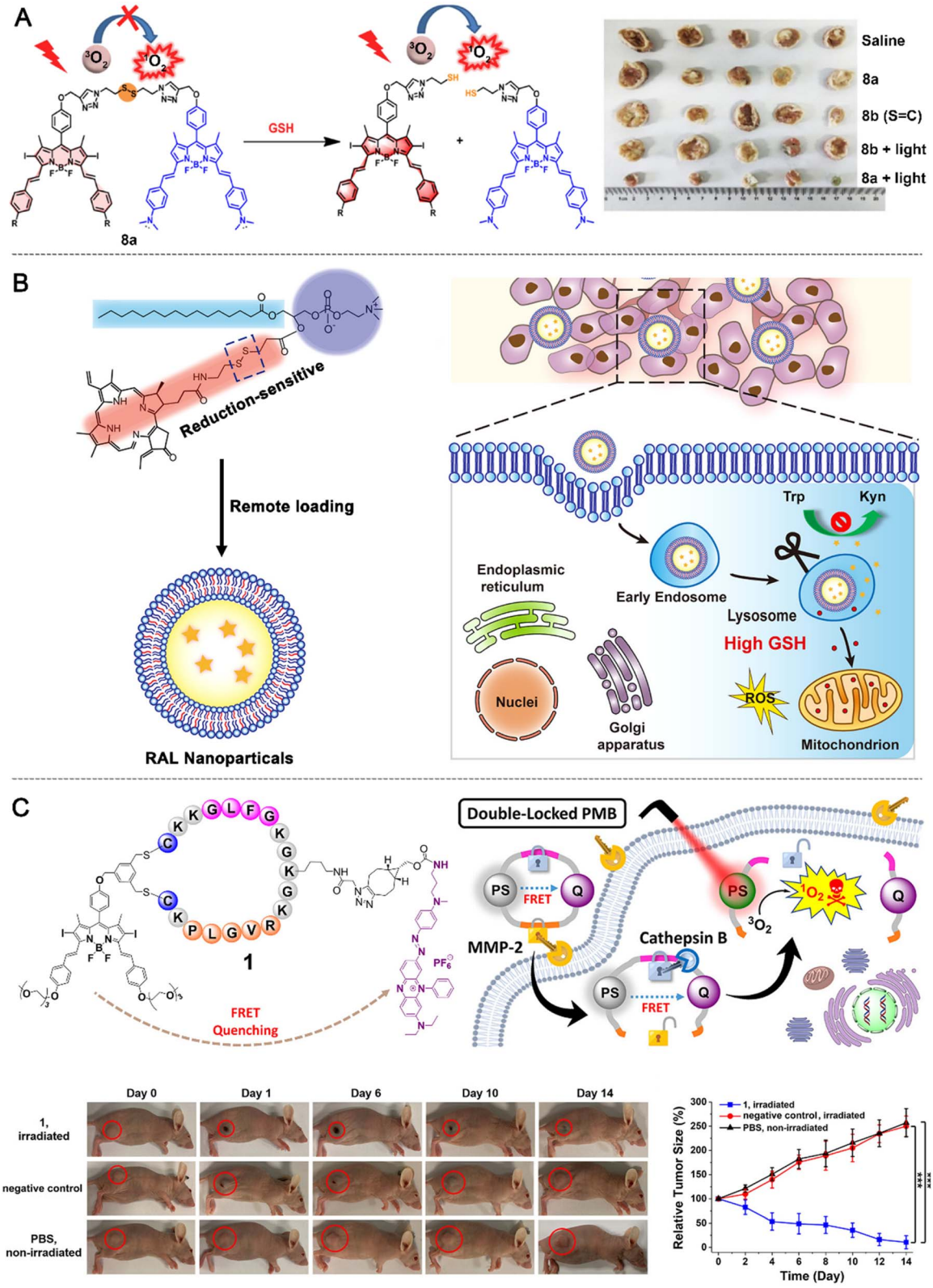

Fig. 3 Examples of FRET based aPS design. (A) GSH responsive FRET aPS design. Reproduced with permission from ref. 59. Copyright 2020, ELSEVIER. (B) Design and mechanism of action of a redox-activated porphyrin-liposome system. Reproduced with permission from ref. 55. Copyright 2019, American Chemical Society. (C) aPS design based on dual-lock FRET quenching. Reproduced with permission from ref. 62. Copyright 2023, American Chemical Society.

© 2026 The Author(s). Published by the Royal Society of Chemistry

Open Access Article. Published on 29 January 2026. Downloaded on 5/27/2026 1:04:59 AM.
This article is licensed under a Creative Commons Attribution-NonCommercial 3.0 Unported Licence.

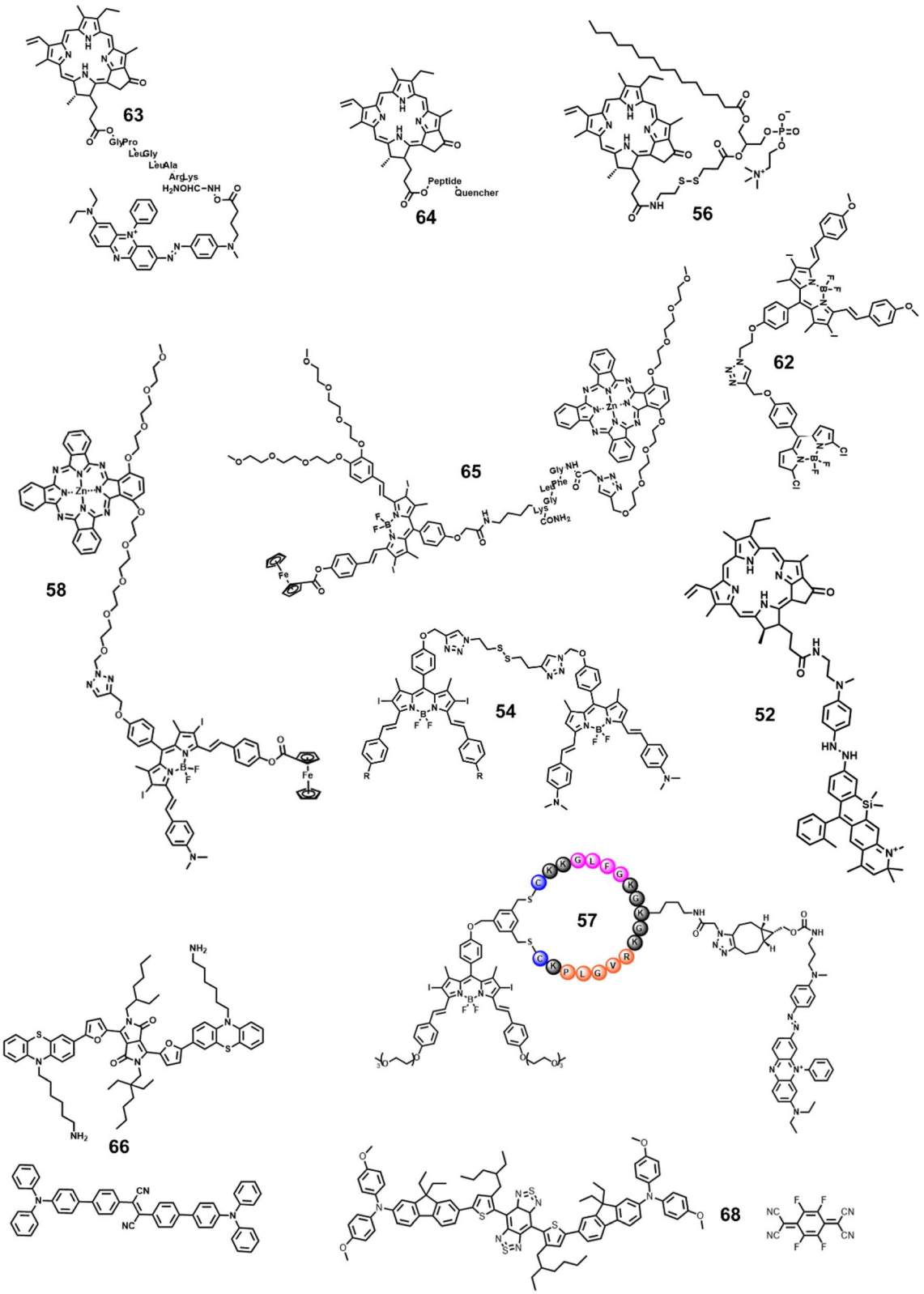

Fig. 4 The main structures of FRET-based aPSs.

complementary strategies for spatially and temporally controlled aPS design. Matrix metalloproteinases (MMPs), a class of zinc-dependent endopeptidases, play a central role in the degradation and remodeling of the extracellular matrix, and their activity is closely associated with tumor invasion, metastasis, and angiogenesis. Because MMPs are markedly overexpressed in a wide range of malignant tumors while being tightly regulated in normal tissues, they are regarded as ideal

Open Access Article. Published on 29 January 2026. Downloaded on 5/27/2026 1:04:59 AM. This article is licensed under a Creative Commons Attribution-NonCommercial 3.0 Unported Licence.

endogenous triggers for achieving precise activation of aPSs within the tumor microenvironment. Based on this biological rationale, Zheng *et al.* first proposed the concept of photodynamic molecular beacons (PMBs) in 2007, successfully realizing MMP-7-dependent, specific regulation of the singlet oxygen-generating capability of photosensitizers.[53] In 2018, Stallivieri and colleagues targeted overexpressed matrix metalloproteinase-2 (MMP-2), MMP-9, and MMP-14 in the TME to design five novel enzyme-responsive PSs, referred to as PMBs.[54] Each PMB consisted of a PS (pyropheophorbide a or P1-COOH), a singlet oxygen quencher (BBQ-650 or BHQ3), and an MMP-cleavable peptide, with some incorporating polyethylene glycol (PEG) spacers to improve solubility and spatial conformation. Optical and photochemical studies showed that in the activatable uncleaved state, FRET efficiently suppressed fluorescence and singlet oxygen generation, achieving optical silence and photodynamic inactivity. Enzymatic assays confirmed that MMP-2 and MMP-14 effectively activated the PMBs, and the PEG spacers further enhanced cleavage efficiency. Subsequent cell experiments demonstrated that the PMBs could be activated by MMPs secreted from tumor cells.

Similarly, Wang *et al.* developed a cathepsin B NQO1(NAD(P)H dehydrogenase (quinone 1))-activatable fluorescent probe and PS (Pc-FcQ) based on a ferrocene-BODIPY dark quencher.[57] The research team first designed and synthesized an iron-based BODIPY quencher featuring broad absorption in the NIR region (500–800 nm) and negligible fluorescence. The introduction of di-triethylene glycol substituents significantly improved its hydrophilicity and biocompatibility. Zinc porphyrin (Pc-COOH) was selected as the fluorophore and photosensitizing unit and conjugated to the quencher through a CTSB-cleavable peptide linker (Gly-Phe-Leu-Gly-Lys) to afford Pc-FcQ. The fluorescence and singlet oxygen generation of the Zn-porphyrin moiety were strongly quenched *via* both FRET and PET, with a fluorescence quenching efficiency of approximately 92% and singlet oxygen yield markedly lower than that of free Pc-COOH. A non-cleavable analogue, N-Pc-FcQ, exhibited similarly quenched optical properties. *In vitro* studies, Pc-FcQ underwent CTSB-mediated peptide cleavage in HepG2 cells, leading to fluorescence recovery. Pre-treatment with a CTSB inhibitor markedly suppressed the fluorescence signal, confirming enzyme-specific activation. Under red-light irradiation, Pc-FcQ showed a lower phototoxic IC_{50} value (0.32 μM) than N-Pc-FcQ (0.53 μM), demonstrating that its photodynamic activity was CTSB-dependent. In *in vivo* experiments, after intratumoral injection into HT29 tumor-bearing nude mice, the fluorescence intensity of Pc-FcQ in the tumor region gradually increased within 10 h, whereas N-Pc-FcQ exhibited only weak fluorescence even after 48 h. These results confirmed that Pc-FcQ could be effectively activated by CTSB *in vivo*. This study broadens the application of dark quenchers in the precise spatiotemporal control of fluorescence and photodynamic activity, providing valuable guidance for the future design of aPSs.

To further improve tumor specificity, Tam *et al.* designed an enzyme-responsive dual-lock PMB (compound 1) to address the low selectivity and skin phototoxicity of conventional PDT[62] (Fig. 3C). The PMB follows an AND logic gate mechanism, requiring sequential cleavage by MMP-2 in the extracellular space (PLGVR substrate) and CTSB in lysosomes (GFLG substrate) to separate the PS DSBDP from the quencher BHQ-3. In its inactive state, FRET completely suppresses fluorescence ($\Phi_F = 0.01$) and ROS generation ($\Phi_\Delta = 0.02$) compared with free DSBDP ($\Phi_F = 0.22$, $\Phi_\Delta = 0.52$). Single-enzyme treatment restored only about 13–16% fluorescence and minimal ROS, while dual-enzyme cleavage produced nearly 85% fluorescence recovery and ROS generation similar to DSBDP. LC-MS confirmed complete conversion to DSBDP and BHQ-3 fragments. In cell studies, strong activation occurred in MMP-2-high tumor cells such as A549 and U-87 MG, whereas weak signals were observed in HeLa and HEK-293 cells with low enzyme expression. ROS detection with H_2DCFDA and light-induced cytotoxicity ($\lambda > 610$ nm, 28 J cm^{-2}) were maximal in dual-enzyme-activated tumor cells (IC_{50} = 0.78–0.91 μM) but much lower in low-expression or inhibitor-treated cells ($IC_{50} \geq$ 3.06 μM). The activated PMB mainly accumulated in lysosomes, consistent with an endocytosis–lysosomal activation process. *In vivo*, intratumoral injection of the PMB into A549 tumor-bearing mice produced strong tumor fluorescence that peaked at 6 h, about 4.3 times higher than that of the non-cleavable control. Light treatment at 680 nm (0.3 W cm^{-2} and 180 J cm^{-2}) significantly inhibited tumor growth without body weight loss or organ toxicity. Notably, the PMB avoided the skin phototoxicity seen with "always-on" DSBDP. This work demonstrates that a dual-enzyme AND gate can achieve high tumor specificity, efficient ROS generation, and minimal off-target toxicity, offering a precise and safe strategy for anticancer PDT and a model for future multi-stimuli-responsive PS design.

FRET-based aPSs offer a versatile and modular strategy for achieving precise control over both fluorescence emission and ROS generation. Beyond enzyme-responsive systems, FRET activation can be rationally coupled to a variety of tumor-associated stimuli, such as acidic pH,[61] redox gradients, hypoxia-induced changes,[52] or specific small biomolecules[60] (*e.g.*, glutathione, hydrogen peroxide, and ATP), to achieve selective activation within the complex TME. The flexibility of FRET allows for the incorporation of diverse recognition motifs and linkers, enabling the construction of programmable aPSs that respond to endogenous biochemical cues or exogenous therapeutic triggers.

Overall, FRET provides (i) spatiotemporal regulation of PS activity through controllable donor–acceptor proximity, (ii) tunable quenching and activation efficiencies *via* spectral and structural optimization, and (iii) the potential implementation of multi-stimuli "AND/OR" logic gates to enhance selectivity and minimize false activation. Moreover, by integrating FRET mechanisms with nanocarriers or supramolecular assemblies, researchers have realized real-time imaging-guided PDT systems that combine diagnostic and therapeutic capabilities in a single platform. By effectively minimizing background fluorescence and off-target phototoxicity, FRET thus establishes a robust foundation for the rational design of next-generation aPSs, representing a key molecular strategy for highly selective, controllable, and clinically translatable tumor-targeted PDT.

© 2026 The Author(s). Published by the Royal Society of Chemistry

Open Access Article. Published on 29 January 2026. Downloaded on 5/27/2026 1:04:59 AM. This article is licensed under a Creative Commons Attribution-NonCommercial 3.0 Unported Licence.

3 PET-based design of aPSs

3.1 Design principles and basic mechanisms

PET is another fundamental mechanism employed in aPSs to regulate photophysical processes at the molecular level. In a PET system, the excited-state energy of a PS is modulated through intramolecular electron transfer between the photosensitizing core and a nearby electron donor or acceptor unit. Unlike FRET, which relies primarily on spatial proximity and spectral overlap, PET efficiency is determined by the redox potentials and frontier orbital energy levels of the interacting components.[69]

Depending on the direction of electron flow, PET can be classified into donor-type (d-PET) and acceptor-type (a-PET) configurations.[70,71] In a-PET, an electron from an electron-rich moiety fills the excited-state vacancy of the PS, thereby deactivating its excited singlet or triplet state. Conversely, in d-PET, the excited PS donates an electron to an electron-deficient group, forming a charge-transfer state that quenches both fluorescence and ROS production. The thermodynamic feasibility of PET is governed by the energy gap between the donor's highest occupied molecular orbital (HOMO) and acceptor's lowest unoccupied molecular orbital (LUMO), which can be finely tuned through chemical modification, conjugation adjustment, or substitution with electron-withdrawing or electron-donating groups.[72]

A typical PET-based aPS consists of a PS core electronically coupled to a responsive recognition unit through covalent or π-conjugated linkage. This regulatory unit serves as an internal quencher, maintaining the molecule in an "off" state until a specific stimulus alters the redox landscape or disrupts the coupling pathway. The resulting change in orbital alignment prevents electron transfer, thereby restoring the PS's excited-state activity (Fig. 5A). For example, Wang *et al.* (2022) developed a NanoPcM nanoprobe, formed by the self-assembly of morpholine-substituted silicon phthalocyanine (PcM) with albumin.[73] Under normoxic conditions, its fluorescence is quenched by the combined effects of PET and ACQ. In the acidic TME, protonation of the morpholine nitrogen removes this quenching and promotes nanoparticle disassembly, thereby activating fluorescence imaging and Type-I PDT. When combined with αPD-1 treatment, NanoPcM further enhances antitumor immunity and induces a strong abscopal effect (Fig. 5B). Based on this principle, a variety of stimulus-responsive systems have also been developed. For example, He *et al.* and Turan *et al.* independently reported phthalocyanine- and BODIPY-based aPSs in which GSH induces the cleavage of electron-donating or "electron-trap" modules, thereby enabling efficient activation within tumor cells. In addition, the PET mechanism has been successfully extended to the sensing of gaseous signaling molecules. Hu *et al.* developed a nitric oxide (NO)-activatable platform that precisely regulates fluorescence imaging and photodynamic therapeutic performance in response to pathological levels of NO.[74–76] Such modular and electronically tunable designs form the basis for constructing PET-based aPSs capable of precise controlled activation through rational molecular engineering (Table 2 and Fig. 7).

3.2 Recent progress in PET-based aPSs

For PET-based aPSs, the design principle relies on PET between an electron donor and an electron acceptor, which can effectively quench fluorescence and suppress singlet oxygen generation under inactive conditions. In this system, the PS can act either as an electron donor (d-PET) or an electron acceptor (a-PET), depending on the electronic properties of the neighboring recognition moiety. Upon encountering specific stimuli, such as changes in pH, redox state, or enzymatic cleavage, the electron transfer process is blocked, restoring the photophysical activity of the PS.

A common PET-based design strategy employs iron-containing ferrocene (Fc) units as electron-donating quenchers. Fc derivatives are attractive due to their strong electron-donating capacity, chemical robustness, and tunable amphiphilicity, making them ideal for constructing PET-based aPSs. By tethering Fc to the PS through cleavable linkers, electron transfer remains active under physiological conditions but is selectively disrupted within pathological microenvironments, thus restoring fluorescence and $^1O_2$ generation. In Lau's work in 2014, the ferrocenyl units function as effective quenchers that suppress both the fluorescence and the singlet oxygen production of the phthalocyanine core *via* the PET mechanism. The design is characterized by the integration of two distinct

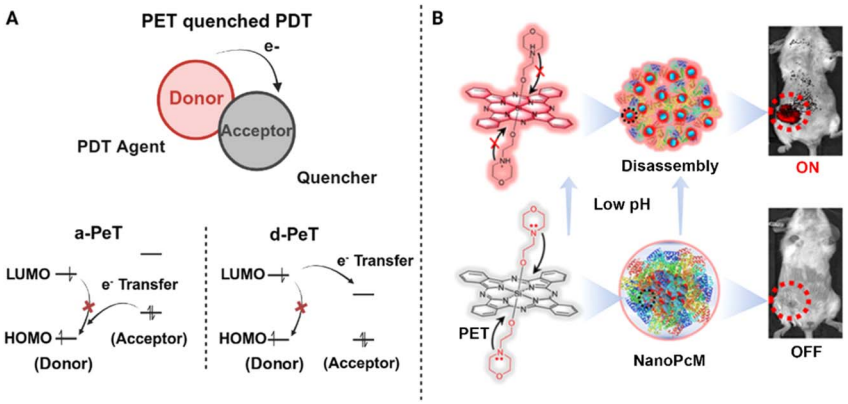

Fig. 5 Basic principle (A) and example (B) of PET based aPS design. Reproduced with permission from ref. 73. Copyright 2022, American Chemical Society.

Open Access Article. Published on 29 January 2026. Downloaded on 5/27/2026 1:04:59 AM. This article is licensed under a Creative Commons Attribution-NonCommercial 3.0 Unported Licence.

Table 2 PET based aPS design

Response factors	Range of stimulation	Response moiety	Photosensitizer	Fluorescence activation	ROS activation	Ref.
GSH	0-1 mM	2,4-Dinitrobenzene sulfonyl moiety	ZnPc	×∼20	—	74
GSH	—	2,4-Dinitrobenzene sulfonyl moiety	BODIPY	—	—	75
NO	0–135 μM	*o*-Phenylenediamine	Bis(phenylethynyl) benzene	×∼45	×100+	76
Hypoxia	0–0.75 μg mL^{-1}	4-Nitrobenzyl	Fluorescein	×7	×∼3.3	77
Hypoxia	0–1 μg mL^{-1}	4-Nitrobenzyl	Cyanine			78
GSH	—	Disulfide bond	TPE	—	—	79
pH	—	Amino group	BODIPY	—	—	80
pH	—	Protonation of the tertiary amine group	TPP (tetraphenylporphyrin)	×2.9	×∼6.1	81
γ-GT	∼100 μM	Acylamide bond	BODIPY	—	—	82
pH	pH 6.0–7.2	Morpholine	Phthalocyanine	—	—	73
GSH	0–10 μg mL^{-1}	Disulfide bond	TPE	—	—	83
ALP	—	Phosphate group	TPA	×126	—	84
Hypoxia	—	Azobenzene linker	AIEgen T-2TM	×7	×1.8	85
Hypoxia	0–10 μg mL^{-1}	4-Nitrobenzyl	Thio-pentamethine cyanine	—	×2.5	86

bioresponsive linkers; specifically, a redox-sensitive disulfide bridge and an acid-labile hydrazone unit were utilized to tether the quenchers to the central photosensitizer. This dual-responsive configuration essentially operates as a molecular logic gate, where the maximum restoration of therapeutic activity is only achieved in environments that are simultaneously acidic and rich in thiols. By demonstrating significantly enhanced *in vitro* photocytotoxicity and successful *in vivo* tumor inhibition, this work validated the utility of ferrocene as a versatile quencher for "smart" theranostics. This pioneering study proved that integrating multiple control elements could drastically reduce non-specific activation, thereby providing the foundational principles for the subsequent evolution of increasingly sophisticated, multi-responsive, and logic-gated photodynamic systems. PET-based aPSs have also been integrated with AIE design principles to circumvent ACQ and minimize nonspecific ROS damage.[87] A representative example based on this work is TPEPY-S-Fc, developed for GSH-activatable, imaging-guided PDT.[79] TPEPY-S-Fc couples an Fc moiety to a TPEPY core *via* a GSH-cleavable disulfide bond. Under normal conditions, PET from Fc effectively quenches TPEPY fluorescence and $^1O_2$ production (Fig. 6A). In tumor cells, elevated GSH cleaves the bond, releasing TPEPY-SH and restricting intramolecular motion, which restores red fluorescence (620 nm, 12-fold enhancement, Φ_F: 0.2% to 10.3%) and $^1O_2$ generation (Φ_Δ: 2.4% to 21.3%), thereby activating both imaging and PDT. Cellular studies revealed mitochondrial accumulation and strong fluorescence in high-GSH cancer cells, but weak emission in normal HUVECs. Upon white-light irradiation (25 μM, 10 min), TPEPY-S-Fc achieved around 90% tumor cell ablation while sparing normal cells, demonstrating its high selectivity and therapeutic precision.

PET-based aPSs have also been engineered to respond to the TME, particularly hypoxia. Conventional PDT suffers from reduced efficacy in oxygen-deficient regions;[88,89] however, the tumor periphery often exhibits mild hypoxia (∼10% O_2), which can be exploited for enzymatic activation. Nitroreductase (NTR)-activatable theragnostic systems based on thermally activated delayed fluorescence (TADF) fluorophores have emerged as effective platforms for fluorescence imaging and PDT under such conditions. Liu *et al.* developed a smart activatable molecule derived from TADF luminophores that undergoes NTR-mediated activation under 10% O_2, enabling efficient fluorescence detection and PDT.[77] The PSs showing superior NTR responsiveness, *in vitro*, demonstrated rapid activation kinetics (completed within 15 min) and high sensitivity (detection limit of 8 ng mL^{-1}). Mechanistic analysis revealed that NTR reduced PSs, suppressing the intramolecular PET process and simultaneously restoring fluorescence and PDT efficiency. Cellular studies confirmed hypoxia-dependent activation, with achieving enhanced PDT efficacy against HeLa cells under 10% O_2 (IC_{50} = 5.91 μM), outperforming protoporphyrin IX (IC_{50} = 6.46 μM). *In vivo*, the PS enabled bright tumor fluorescence imaging and significantly inhibited tumor growth in HeLa-bearing mice. This study demonstrates the strategic use of mild hypoxia at tumor margins as an activation trigger, effectively overcoming the limitations of conventional PDT under severe hypoxia and integrating diagnostic and therapeutic functions in a single design.

Building on the concept of mild hypoxia-activated PET-based aPSs, Zheng *et al.* reported a NIR theranostic PS, CYNT-1, derived from a trimethylammonium phthalocyanine dye.[78] CYNT-1 is activated by NTR under mild hypoxia, enabling selective fluorescence imaging and efficient PDT. The molecule was constructed by introducing a 4-nitrobenzyl group into CYNT, a phthalocyanine dye with a long triplet-state lifetime (9.16 μs), where fluorescence and PDT efficiency remained "off" due to intramolecular PET. CYNT-1 exhibited high selectivity

© 2026 The Author(s). Published by the Royal Society of Chemistry

Open Access Article. Published on 29 January 2026. Downloaded on 5/27/2026 1:04:59 AM.
This article is licensed under a Creative Commons Attribution-NonCommercial 3.0 Unported Licence.

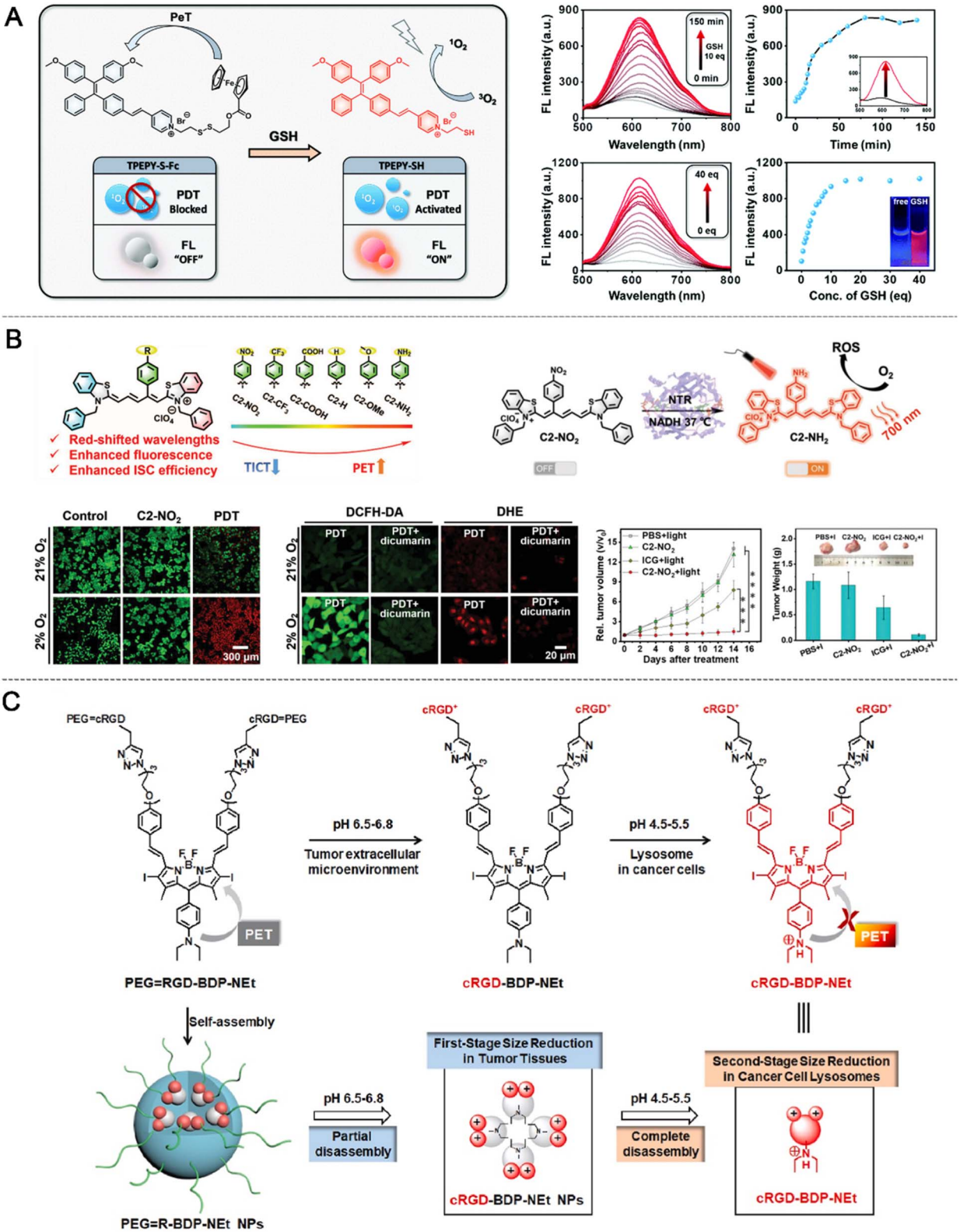

Fig. 6 Examples of PET based aPS design. (A) GSH responsive PET aPS design. Reproduced with permission from ref. 79. Copyright 2020, The Royal Society of Chemistry. (B) Mechanistic study on the regulation of C2′-substituted TCy5 derivatives. Reproduced with permission from ref. 86. Copyright 2024, Wiley-VCH GmbH. (C) Nano-to-molecular disassembly aPS design. Reproduced with permission from ref. 80. Copyright 2021, Elsevier.

Open Access Article. Published on 29 January 2026. Downloaded on 5/27/2026 1:04:59 AM.
This article is licensed under a Creative Commons Attribution-NonCommercial 3.0 Unported Licence.

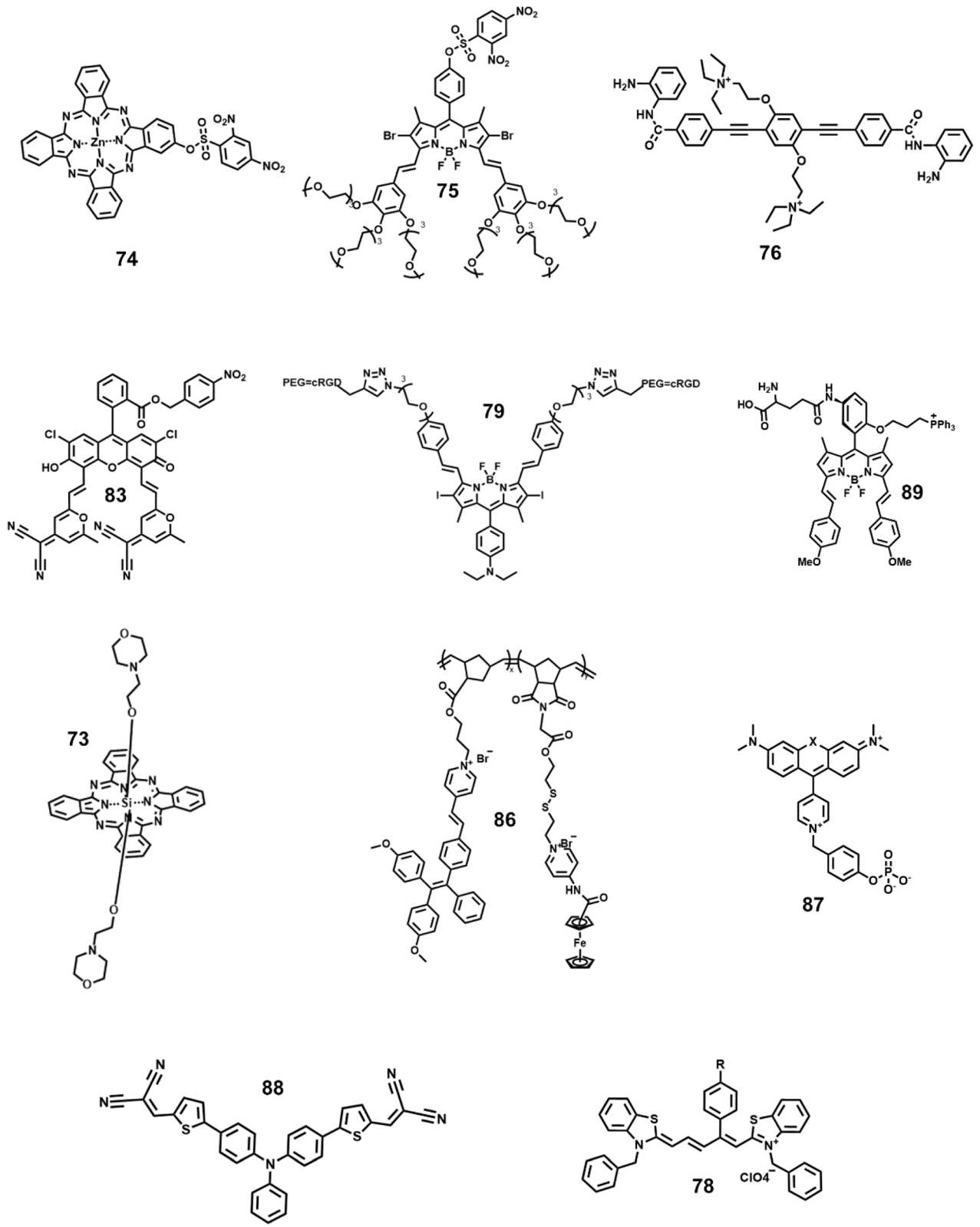

Fig. 7 The main structures of PET-based aPSs.

toward NTR (detection limit 16 ng mL^{-1}) and rapid activation within 15 min. In cell studies, CYNT-1 showed strong hypoxia-dependent activation and optimal PDT efficacy against HeLa cells under varying hypoxic conditions. Using 3D spheroid models to mimic the TME, CYNT-1 penetrated up to 160 μm and was activated within the spheroids. Mechanistic studies indicated lysosomal targeting, where $^1O_2$ generation disrupted lysosomal integrity and induced apoptosis. This represents the

© 2026 The Author(s). Published by the Royal Society of Chemistry

Open Access Article. Published on 29 January 2026. Downloaded on 5/27/2026 1:04:59 AM. This article is licensed under a Creative Commons Attribution-NonCommercial 3.0 Unported Licence.

first NIR-range NTR-activatable theragnostic molecule, overcoming the limited tissue penetration of visible-light-based agents and providing a promising strategy for integrated diagnosis and therapy of deep tumor tissues.

Although these aPSs display favorable photophysical properties, more advanced molecular regulation strategies are needed to address the challenges of clinical applications under varying conditions. Peng *et al.* reported a series of C2′-substituted TCy5 derivatives, including C2-NO_2 and C2-NH_2, as NTR-aPSs for hypoxia-targeted PDT.[86] The dyes were synthesized *via* a three-step strategy introducing electron-withdrawing groups (*e.g.*, –NO_2 and –CF_3) or electron-donating groups (*e.g.*, –OMe and –NH_2) at the C2′ position (Fig. 6B). These substitutions modulate twisted intramolecular charge transfer (TICT) and PET: electron-withdrawing groups enhance TICT and quench fluorescence, whereas electron-donating groups reduce TICT, strengthen PET, and simultaneously improve Φ_F and intersystem crossing (ISC) efficiency. Under hypoxic tumor conditions, C2-NO_2 is reduced by NTR to C2-NH_2, restoring photophysical activity. *In vitro* characterization using UV-vis-NIR absorption, fluorescence spectroscopy, diphenylisobenzofuran assay, and electron spin resonance confirmed $^1O_2$ generation, ROS type, and excited-state dynamics, with femtosecond transient absorption revealing rapid excitation processes. Cellular studies showed that HepG2 cells under hypoxia exhibited a 4.9-fold fluorescence increase compared with normoxia, and 660 nm irradiation (20 mW cm^{-2}, 15 min) reduced tumor cell viability below 20% while sparing normal cells (>70% survival). C2-NO_2 preferentially localized in mitochondria (Pearson's $r = 0.91$). In BALB/c mice bearing 4T1 xenografts, intratumoral injection of C2-NO_2 produced peak fluorescence within 3 h, and combined 671 nm irradiation (100 mW cm^{-2}, 15 min) over 14 days limited tumor growth to 1.5-fold, outperforming indocyanine green controls, without observable toxicity. This C2′-substituted TCy5 platform overcomes the conventional trade-off between fluorescence and ISC efficiency in cyanine dyes, providing a tunable molecular strategy for hypoxia-responsive fluorescence-guided PDT and a promising avenue for precise tumor theranostics.

Beyond redox and hypoxia responsiveness, tumor tissues and intracellular compartments also exhibit significant acidification, providing an opportunity for pH-responsive regulation of aPSs. Zhang *et al.* developed PEG = R-BDP-NEt NPs based on BDP, in which PEG and cRGD-BDP-NEt were linked *via* a Schiff base to form dual-stage pH-responsive nanoparticles.[80] Under mildly acidic extracellular conditions (pH ≈ 6.5), the PEG shell hydrolyzed to expose cRGD, enabling $\alpha_v\beta_3$ targeting (Fig. 6C). Upon lysosomal entry (pH ≈ 4.5), protonation of the NEt group blocked PET, triggering complete nanoparticle disassembly and restoring strong fluorescence and photosensitivity. The system showed potent phototoxicity toward tumor cells at pH 6.5 ($IC_{50} = 0.8$ μM), significantly lower than that under neutral conditions, and achieved substantial tumor growth inhibition *in vivo* (tumor growth inhibition ≈ 85%) without systemic toxicity. To further enhance the precision and multifunctionality of aPS delivery systems, Zhang and colleagues, building on a stepwise activation strategy, designed a sequentially responsive polypeptide-based nanoplatform (PPTP@PTX2 NPs) to achieve synergistic PDT and chemotherapy.[81] This system was constructed by encapsulating a diselenide-linked paclitaxel dimer prodrug (PTX2) within acid-activatable polypeptide micelles, whose surface was functionalized with tetraphenylporphyrin (TPP) photosensitizers and cRGD targeting ligands. Under physiological pH conditions, TPP molecules confined within the micellar state remain quenched due to the combined effects of PET and ACQ. Upon accumulation in the acidic tumor microenvironment or lysosomes (pH ≈ 5.0), protonation of the micellar core triggers micelle disassembly, thereby restoring the fluorescence and photodynamic activity of TPP. Subsequently, the elevated intracellular GSH levels further cleave the diselenide bonds in the prodrug, releasing bioactive paclitaxel. This acidity-initiated and redox-regulated sequential activation strategy not only markedly reduces off-target toxicity but also achieves exceptionally high tumor inhibition in breast cancer models. As such, it provides an effective paradigm for the construction of highly controllable multimodal therapeutic platforms.

Overall, PET-based activation provides a highly flexible and universal molecular regulation framework for the precise design of aPSs. By incorporating electron donor or acceptor units that respond to external stimuli (such as pH, ionic strength, polarity changes, or molecular recognition events), PET enables controllable "on/off" switching of fluorescence and photoreactivity at the molecular level. This allows aPSs to achieve higher selectivity and signal-to-noise ratios in complex biological environments, effectively avoiding the high background and nonspecific phototoxicity seen in "always-on" systems. Beyond pH, PET has been applied to various responsive modalities, including enzyme catalysis (such as NTR, β-gal, and γ-GT), redox potential, viscosity, and hypoxia.[83–85] Recent advances include PET-regulated hypoxia-responsive systems for promoting cancer immunotherapy and heavy-atom-free platforms for real-time *in situ* monitoring of therapeutic feedback.[82] Coupling these mechanisms with specific physiological or pathological signals enables precise visualization and regulation of tumors, inflammation, and metabolic states. In summary, PET is not only one of the most fundamental and versatile molecular control strategies in aPS design, but also provides a foundation for developing intelligent photosensitizing systems that integrate diagnostic and therapeutic functions.

4 ICT-based design of aPSs

4.1 Design principles and basic mechanisms

ICT occurs in molecules that contain an electron donor and an electron acceptor linked by a π-conjugated bridge.[90] When these molecules absorb light, electrons move from the donor to the acceptor, forming a polarized excited state. The extent of this charge movement depends on molecular features such as conjugation length, planarity, and the electronic nature of substituents.[91] ICT efficiency is also influenced by the spatial relationship between the donor and acceptor. Factors such as bond rotation, torsion, and local flexibility affect orbital overlap, which determines whether the excited energy is released as light or dissipated through non-radiative pathways.[92,93] By adjusting

Open Access Article. Published on 29 January 2026. Downloaded on 5/27/2026 1:04:59 AM. This article is licensed under a Creative Commons Attribution-NonCommercial 3.0 Unported Licence.

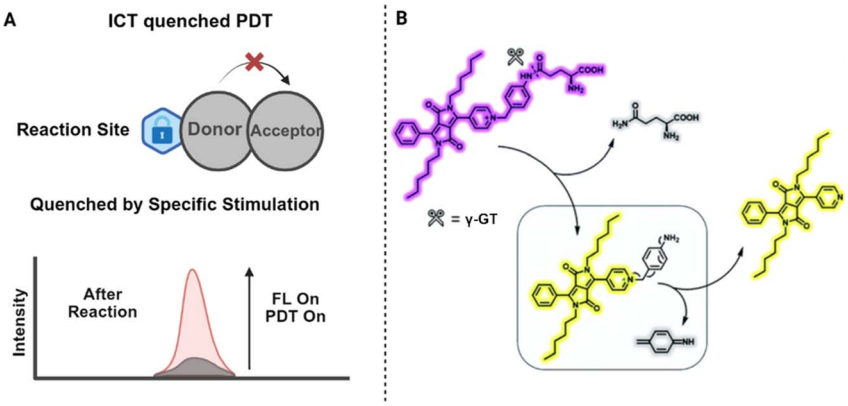

Fig. 8 Basic principle (A) and example (B) of ICT based aPS design. Reproduced with permission from ref. 94. Copyright 2020, The Royal Society of Chemistry.

these parameters, researchers can regulate the fluorescence intensity and ROS generation efficiency of PSs.

In a typical ICT-based aPS, the donor and acceptor units are electronically connected, and their interaction can be switched on or off by environmental cues. A regulatory group may temporarily block the charge transfer process, keeping the molecule in an inactive state under normal conditions. When disease-related stimuli such as enzyme action, pH variation, or redox imbalance occur, this group is removed or transformed and the ICT pathway is restored (Fig. 8A). The molecule then regains its fluorescence and photodynamic activity. A representative example can be seen in the work reported by Yang *et al.* in 2020.[94] In this study, the authors designed the probe DPP-Γ-GT based on a diketopyrrolopyrrole (DPP) core and introduced a γ-glutamyl group to target γ-glutamyl transpeptidase (Γ-GT). The ICT effect gives the probe red fluorescence. After Γ-GT specifically cleaves the amide bond, the ICT process is blocked, causing the fluorescence to shift to yellow and simultaneously activating the PS DPP-py (Fig. 8B). This design enables selective PDT toward HepG2 cells with high Γ-GT expression. This design principle provides a flexible strategy for building ICT-based aPSs. It allows precise control of photoactivation behavior and enables selective ROS generation in diseased tissues while maintaining low background activity in healthy environments (Table 3 and Fig. 10).

4.2 Recent progress in ICT-based aPSs

The ICT process relies on the redistribution of electron density between donor (D) and acceptor (A) units within a molecule, and enzymes, due to their excellent substrate selectivity, often serve as effective triggers in ICT-based aPS designs.[109] γ-Glutamyl transpeptidase (Γ-GT), a membrane-associated enzyme upregulated in various tumors, provides a tumor-specific trigger for ICT-based aPS.[110] Incorporating γ-glutamyl moieties into the PS suppresses fluorescence and ROS generation until enzymatic cleavage restores the ICT pathway. Liu *et al.* developed CyI-Glu, in which a NIR cyanine fluorophore (CyI-OH) was masked by a γ-glutamyl group *via* a 4-amino-benzyl alcohol linker.[99] Without Γ-GT, the probe showed negligible fluorescence and ROS generation. In tumor cells with high Γ-GT expression, the γ-glutamyl group was cleaved, releasing CyI-OH and inducing a 38-fold fluorescence enhancement at 718 nm and efficient $^1O_2$

Table 3 ICT based aPS design

Response factors	Range of stimulation	Response moiety	Photosensitizer	Fluorescence activation	ROS activation	Ref.
Hypoxia	—	4-Nitrobenzyl	Hemicyanine	—	×2.5	95
CTSB	—	Peptide	BODIPY	—	—	96
CTSB	—	Peptide	Hemicyanine	—	—	97
γ-GT	0–200 U L^{-1}	γ-Glutamyl	Diketopyrrolopyrrole	×80	—	94
γ-GT	80 U L^{-1}	γ-Glutamyl	Rhodamine	×7	×∼3.3	98
γ-GT	0–60 U L^{-1}	γ-Glutamyl	Synthesized	—	—	99
β-Gal	0–5 U	Glycosidic linkage	Resorufin	×22	—	100
ALP	1 U L^{-1}	Phosphate group	Hemicyanine	×21.3	×3.8	101
Hypoxia	0.2 μg mL^{-1}	2-Nitroimidazole	Synthesized	—	—	102
NQO1	3.4 μg mL^{-1}	Quinone	DSBDP	×45	—	103
NQO1	0–10 μg mL^{-1}	Quinone	Bromic cyanine	—	—	104
NQO1	0.05–1.5 μg mL^{-1}	Quinone	Hemicyanine	—	—	105
H_2O_2	—	Boronic acid	Ir(III) phenylpyridine	—	—	106
ALP	0–120 U L^{-1}	Phosphate group	Hemicyanine	—	—	107
Hypoxia	0–10 μg mL^{-1}	2-Methoxy-4-nitrophenyl	Benzophenothiazine	—	×∼4	108

© 2026 The Author(s). Published by the Royal Society of Chemistry

Open Access Article. Published on 29 January 2026. Downloaded on 5/27/2026 1:04:59 AM.
This article is licensed under a Creative Commons Attribution-NonCommercial 3.0 Unported Licence.

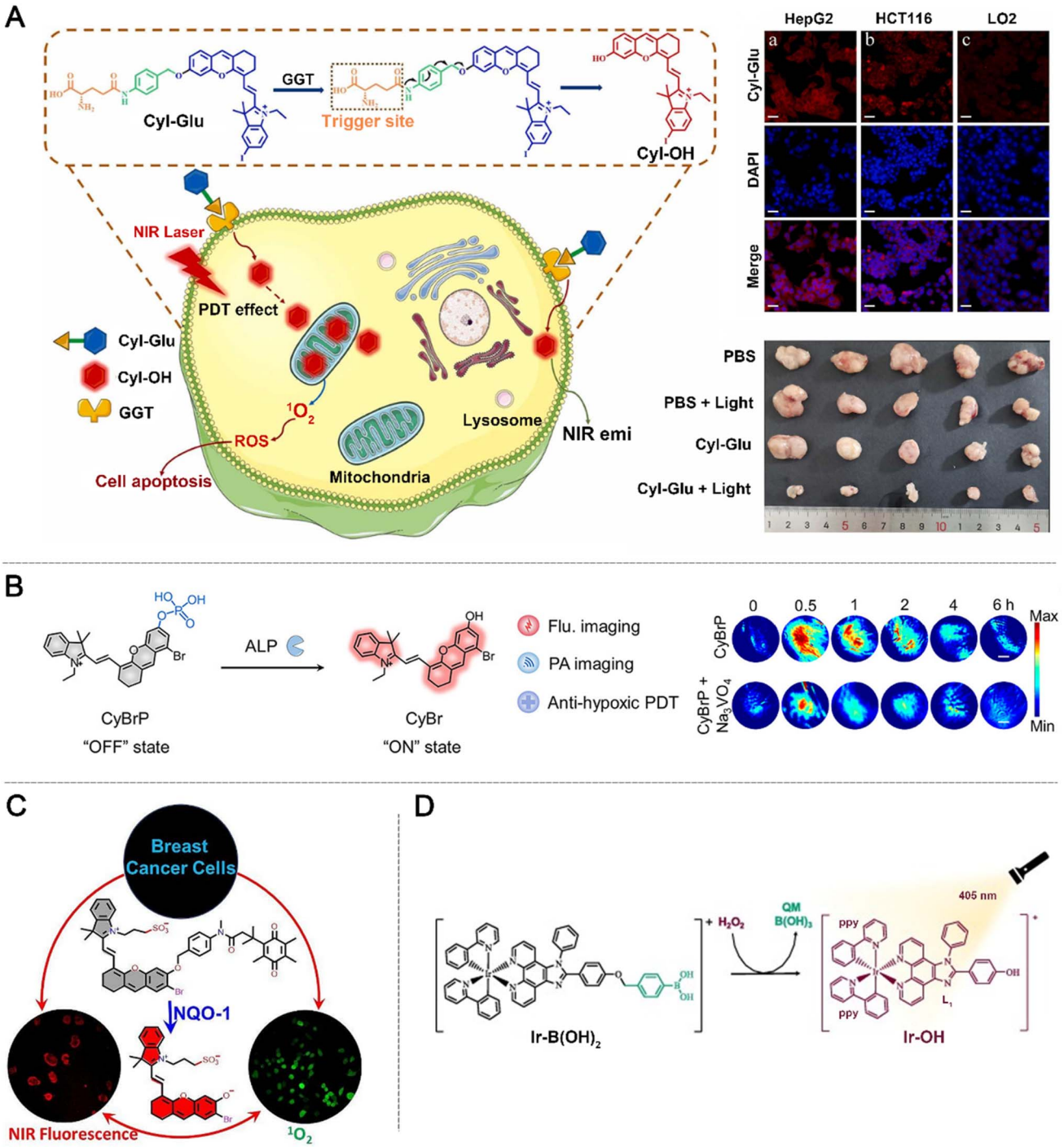

Fig. 9 Examples of ICT based aPS design. (A) γ-Γ-GT responsive ICT aPS design. Reproduced with permission from ref. 99. Copyright 2022, Elsevier. (B) ALP responsive ICT aPS design. Reproduced with permission from ref. 101. Copyright 2023, American Chemical Society. (C) NQO-1 responsive ICT aPS design. Reproduced with permission from ref. 105. Copyright 2024, Elsevier. (D) H_2O_2-responsive Ir(III) PS design based on density functional theory (DFT) calculations. Reproduced with permission from ref. 106. Copyright 2024, Elsevier.

generation under 690 nm irradiation (Fig. 9A). The detection limit was as low as 0.014 U L^{-1}, and cell studies showed selective phototoxicity, with over 80% of HepG2 tumor cells killed under light, while normal LO2 hepatocytes remained largely unaffected. Similarly, Li *et al.* introduced Glu-RdEB, a multifunctional construct linking a rhodamine fluorophore and the ENBS PS *via* a self-degradable arm.[98] The γ-glutamyl group blocked rhodamine fluorescence and ENBS photoreactivity. Enzymatic cleavage in Γ-GT-overexpressing cells restored rhodamine fluorescence (580–650 nm) for imaging and activated ENBS to generate O_2^- under 660 nm light. This system achieved 90% tumor cell killing in U87 cells at 0.4 μM, while sparing normal hepatocytes. Collectively, these Γ-GT-activated ICT-type aPSs demonstrate excellent selectivity, low detection

Open Access Article. Published on 29 January 2026. Downloaded on 5/27/2026 1:04:59 AM.
This article is licensed under a Creative Commons Attribution-NonCommercial 3.0 Unported Licence.

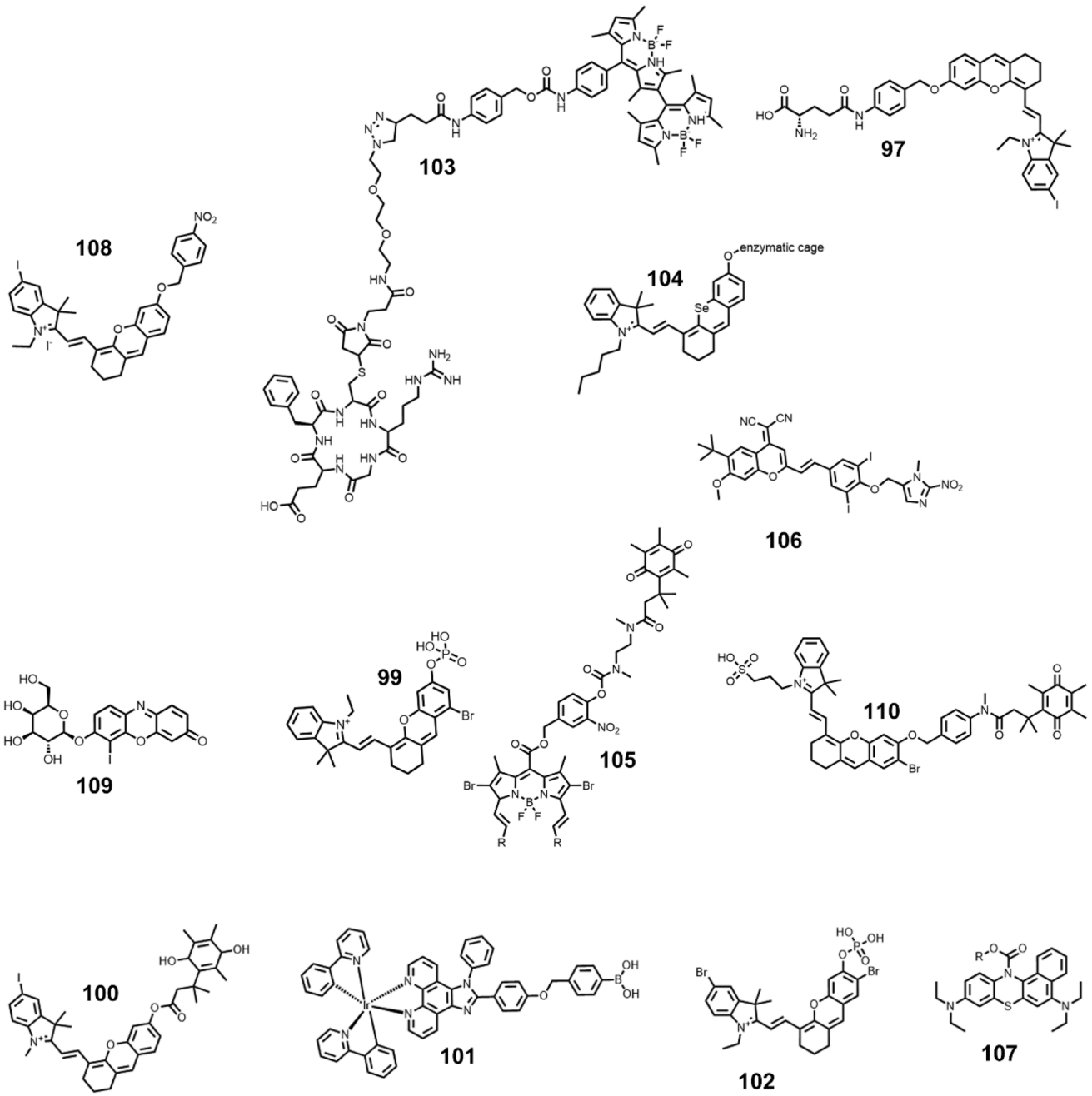

Fig. 10 The main structures of ICT-based aPSs.

limits, and strong therapeutic efficacy, highlighting ICT modulation as a robust strategy for enzyme-specific, image-guided PDT.

The ICT strategy can also be extended to other tumor-associated enzymes, such as ALP, which is overexpressed in various cancers and serves as a promising trigger for aPSs. Zhang *et al.* employed a phthalocyanine core and a halogen-substitution strategy, synthesizing four derivatives: CyH, CyBro, CyBr, and CyI. DFT calculations confirmed that Br/I introduction increased spin–orbit coupling constants (CyBr: 0.24 cm^{-1}), accelerating ISC while suppressing $^1O_2$ generation and promoting Type I ROS production.[101] An ALP-responsive probe, CyBrP, was constructed based on CyBr, in which a phosphate group blocked the ICT effect (Fig. 9B). In the inactive state, fluorescence and phototoxicity were negligible. ALP-mediated hydrolysis released CyBr, resulting in 21.3-fold NIR fluorescence enhancement and a 12.5-fold increase in the photoacoustic signal. In HepG2 cells and tumor-bearing mice, CyBrP enabled efficient PDT under both normoxic and hypoxic conditions, achieving 90% tumor growth inhibition without organ toxicity. Building on this halogen-substitution strategy, Zhao *et al.* (2024) incorporated fluorescence upconversion luminescence technology to overcome limited light penetration in deep tumors.[107] NFh-Br derivatives were synthesized on a phthalocyanine scaffold, with doubly brominated NFh-Br_{11} exhibiting excellent fluorescence upconversion luminescence

© 2026 The Author(s). Published by the Royal Society of Chemistry

Open Access Article. Published on 29 January 2026. Downloaded on 5/27/2026 1:04:59 AM. This article is licensed under a Creative Commons Attribution-NonCommercial 3.0 Unported Licence.

performance (emission at 735 nm) and $^1O_2$ generation efficiency (diphenylisobenzofuran degradation of 97.5% in 15 min) under 808 nm excitation. The ALP-responsive probe NFh-ALP used phosphate caging to remain inactive until ALP hydrolysis released NFh-Br_{11}, enabling lysosomal targeting in A549/HeLa cells (Pearson coefficient of 0.92) and reducing cell viability below 40% at 10 μM. *In vivo*, 808 nm light-guided tumor fluorescence confirmed selective accumulation, and treatment achieved complete tumor suppression with favorable biosafety. Collectively, these studies demonstrate the versatility of ALP-responsive ICT-based aPSs, highlighting the combination of halogen substitution and enzyme-triggered activation as a powerful strategy for precise PDT in hypoxic tumors and advancing the potential for clinical translation.

Other tumor-specific enzymes have also attracted attention. Lu *et al.* (2020) addressed the nonspecific toxicity and low therapeutic efficiency of conventional PSs by developing a CTSB-activatable aPS (ABP) based on BODIPY dimers.[96] A CTSB-specific cleavable peptide (Gly-Phe-Leu-Gly) was conjugated to a BODIPY dimer (BDP-BDP-NH_2), in which the peptide blocked the amino group, suppressing ICT and markedly reducing $^1O_2$ production. To enhance tumor targeting and drug-loading capacity, ABP was further modified with PEG and the cRGD peptide. This construct effectively encapsulated the hydrophobic chemotherapeutic 10-hydroxycamptothecin (HCPT), forming stable RNC/HCPT nanoparticles (~200 nm) with excellent serum stability, providing a multifunctional platform for enzyme-triggered imaging and combined chemo-photodynamic therapy. *In vitro* studies with 4T1 cells demonstrated that CTSB cleaved the peptide linker, restoring the ICT effect of BDP-BDP-NH_2. Upon 488 nm irradiation, $^1O_2$ generation increased significantly. The cRGD modification facilitated nanoparticle binding to $\alpha_v\beta_3$ integrin, enhancing cellular uptake. Combination PDT and chemotherapy induced 48.8% cell death, compared with only 15.9% for chemotherapy alone. In 4T1 3D tumor spheroids, RNC/HCPT penetrated to the spheroid core, and subsequent laser irradiation caused marked spheroid shrinkage and structural disruption, validating the system in a tumor-mimicking environment and establishing a model for enzyme-activatable combinational therapy. To overcome the limitations of BODIPY-based systems in NIR responsiveness and *in vivo* safety, Cheng *et al.* developed a Se-bridged phthalocyanine-based CTSB-activatable NIR aPS.[97] The Se atom's heavy-atom effect enhanced ISC, enabling efficient $^1O_2$ generation in the 700–800 nm NIR-I window. ICT was blocked *via* phenol hydroxyl caging (methoxy protection) to minimize off-target phototoxicity. A CTSB-responsive peptide (Val-Cit/GFLG) was conjugated to the Se-phthalocyanine *via* a self-degrading 4-aminobenzyl alcohol linker, and PEGylation improved solubility, yielding compound 18. In U87 cells, enzymatic cleavage released the active PS, while inhibition with E-64 significantly reduced fluorescence and phototoxicity. In zebrafish bearing U87 microtumors, 720 nm irradiation with compound 18 reduced tumor volume by >60% without affecting morphology, heartbeat, or motility. This work demonstrates that optimizing organic scaffolds *via* Se-bridging and modular design addresses NIR penetration and *in vivo* safety, providing a promising strategy for enzyme-activatable NIR aPSs in clinical applications.

Expanding on enzyme-activatable ICT strategies, NQO1 has emerged as a valuable tumor-specific trigger due to its high expression in various solid tumors. ICT-based aPSs activated by NQO1 enable spatiotemporal control of photodynamic activity, minimizing off-target damage. Cao *et al.* (2024) addressed the limitations of conventional PSs, including poor targeting, low PDT efficiency, and weak immune responses, by developing a NIR multifunctional theranostic probe, I-HCy-Q.[105] The probe employs iodine-substituted phthalocyanine (I-HCy) as the fluorescent and photosensitizing core, with an NQO1-specific recognition group directly conjugated to suppress ICT (Fig. 9C). In the inactive state, fluorescence ($\lambda_{ex/em}$ = 685/703 nm) and $^1O_2$ generation are minimal. I-HCy-Q exhibits a linear NQO1 detection range of 0.05–1.5 μg mL^{-1}, a detection limit of 5.66 ng mL^{-1}, and excellent selectivity and pH tolerance. In NQO1-positive A549 and 4T1 cells, enzymatic activation released I-HCy, which localized to mitochondria (Pearson coefficient of 0.902). Under 660 nm light, substantial ROS production induced mitochondrial membrane depolarization and cytochrome c release, with apoptosis reaching 74.8% (early 22.4% + late 52.4%) after 20 min of irradiation. Notably, mitochondrial-targeted PDT triggered ICD, promoting calreticulin exposure, HMGB1 secretion, and ATP release, providing a foundation for combination immunotherapy. *In vivo*, intratumoral injection in 4T1 tumor-bearing mice produced strong fluorescence within 30 min, which was significantly diminished by pre-treatment with the NQO1 inhibitor dicoumarol, confirming enzyme-specific activation. Beyond mitochondrial targeting, NIR-activated aPSs improve tissue penetration for deeper tumor therapy. Xue *et al.* developed a far-red light-responsive BODIPY-based PS in which photodynamic activity was caged by an ester group.[103] NQO1-catalyzed two-electron reduction of quinone, coupled with self-immolative linker cleavage, converted the ester to a carboxylate, restoring ICT and PDT activity. Post-activation, the absorption maximum shifted to 652 nm, fluorescence quantum yield increased from 0.026 to 0.59, and $^1O_2$ quantum yield rose from 0.03 to 0.15. At the cellular level, the probe selectively activated NQO1-positive A549 and HT29 cells (fluorescence is 5–8× higher than that of NQO1-negative HUVECs), with phototoxic IC_{50} values of 5.56 μM and 4.65 μM, predominantly *via* apoptosis. In HT29 tumor-bearing mice, intratumoral activation was confirmed, with fluorescence peaking at 24 h. These studies collectively demonstrate that NQO1-activatable ICT aPSs offer precise tumor targeting, efficient ROS generation, and NIR compatibility, providing a robust platform for enzyme-guided, image-assisted PDT with potential immunotherapeutic synergy.

Designing aPSs responsive to TME stimuli is a crucial strategy to enhance the precision and hypoxia adaptability of PDT. Barretta *et al.* approached this from a theoretical perspective, developing H_2O_2-responsive Ir(III) complexes (IrOH) and optimizing their structures using DFT and time-dependent density functional theory calculations to maximize the therapeutic window[106] (Fig. 9D). By introducing π-conjugated electron donors such as *N*,*N*-dimethyl-*N*-ethylvinylamine (dmva) or

Open Access Article. Published on 29 January 2026. Downloaded on 5/27/2026 1:04:59 AM. This article is licensed under a Creative Commons Attribution-NonCommercial 3.0 Unported Licence.

methoxyvinyl (mv) into the 2-phenylpyridine (ppy) ligand, or substituting the metal center with isoelectronic Os(II), absorption was red-shifted: Ir_1/Ir_2 exhibited elevated HOMO levels and narrower gaps, with absorption at 560–598 nm, while OsOH reached 780 nm in the NIR region. The heavy atom effect enhanced spin–orbit coupling, ensuring ISC efficiency and $^1O_2$ generation (T_1 energy is 1.31 eV > 0.93 eV O_2 excitation threshold), while avoiding Type I ROS pathways, providing computational guidance for metal-based stimulus-responsive aPS design.

Hypoxia is a characteristic feature of solid tumors that significantly limits the therapeutic efficacy of traditional oxygen-dependent PDT. Consequently, engineering hypoxia-activatable systems has emerged as a key strategy to improve treatment selectivity and overcome oxygen-related resistance in deep-seated tumors.[78,102] Zeng *et al.* addressed hypoxic tumor therapy limitations by developing an NTR-activatable, fully caged Type I pro-PS, BPN2, demonstrating translation from theoretical design to preclinical application.[108] BPN2 incorporates benzo [*b*]phenothiazine (BP) as the Type I PS core, linked *via* a carbamate to 2-methoxy-4-nitrophenyl as the NTR-responsive moiety. In its inactive state, BP's conjugation is disrupted, exhibiting no NIR absorption (500–800 nm) or photoreactivity. Under hypoxic tumor conditions with elevated NTR, the nitro group is reduced to an amine, releasing free BP and restoring 680 nm absorption, 705 nm fluorescence (detection limit is 5.66 ng mL^{-1}), and superoxide (O_2^-) generation (DHR123 fluorescence is enhanced 3.1×). Notably, single-pulse 680 nm laser irradiation allows BPN2 to trigger simultaneous Type I PDT (oxidative damage) and photoacoustic cavitation (mechanical damage). *In vitro*, EMT6 cells under $CoCl_2$-simulated hypoxia treated with 25 μM BPN2 plus laser showed 28.3% survival and 78.36% apoptosis. In EMT6 tumor-bearing mice, tail vein injection achieved a tumor signal-to-background ratio of 54.3 at 12 h, and 18-day combined therapy resulted in 92.1% tumor inhibition without cardiac or hepatic toxicity. This enzyme-activated, dual-effect synergistic design overcomes the hypoxia sensitivity and nonspecific toxicity of traditional PDT, offering a translatable approach for precise treatment of hypoxic solid tumors.

ICT-based aPSs offer a highly adaptable strategy for achieving precise control over both fluorescence emission and ROS generation. By modulating the electronic coupling between donor and acceptor units, ICT enables stimulus-responsive activation in response to a wide range of pathological cues, including enzymatic activity, pH changes, redox imbalance, and reactive oxygen/nitrogen species. Careful molecular design—through adjustment of conjugation length, planarity, and substituent electronics—allows fine-tuning of activation efficiency, photodynamic output, and temporal response, while maintaining minimal background activity in healthy tissues. Moreover, ICT can be integrated with multifunctional nanocarriers or supramolecular assemblies to achieve real-time imaging-guided PDT, combining diagnostic and therapeutic functions in a single platform. By providing precise, selective, and tunable control over PS activity, ICT establishes a robust framework for the rational design of next-generation aPSs, advancing the development of highly selective, controllable, and clinically translatable tumor-targeted PDT.

5 ACQ-based design of aPSs

5.1 Design principles and basic mechanisms

ACQ is a common photophysical process observed in many PSs, which can be used to design activatable systems for PDT. Most PSs have planar and hydrophobic molecular frameworks that tend to aggregate in aqueous environments. When aggregation occurs, strong intermolecular interactions form non-emissive ground-state complexes. As a result, both fluorescence and singlet oxygen generation are suppressed. This quenching behavior can be deliberately integrated into molecular design. Multiple PS molecules can be assembled into nanoparticles or supramolecular aggregates, remaining in an inactive state during circulation. Such assemblies show minimal background fluorescence and negligible phototoxicity under physiological conditions.

Activation takes place when pathological cues induce disassembly or structural rearrangement of the aggregates. Stimuli such as enzymatic cleavage, pH variation, or redox imbalance can disrupt molecular packing and restore the monomeric form of the PS.[111] Once disassembled, the molecules recover their fluorescence and ROS generation ability (Fig. 11A). A classic design can be seen in the study reported by Chu *et al.* in 2024. In this work, the authors developed the nanoPS Gal-$(ZnPc^*)_2$ by linking a dimeric zinc phthalocyanine with a β-galactose unit and a self-immolative linker.[112] The conjugate self-assembles into nanoparticles in aqueous solution, where both fluorescence and singlet oxygen generation are quenched (Fig. 11B). After entering senescent cells, β-galactosidase cleaves the glycosidic bond, triggering self-immolation and releasing the active monomer. This process enables fluorescence imaging and photodynamic eradication of senescent cells.

ACQ-based aPSs provide a simple and reliable design strategy for spatially and temporally controlled activation (Table 4 and Fig. 13). By confining photodynamic activity to diseased regions and minimizing collateral damage in normal tissues, this approach improves therapeutic precision and overall biosafety.

5.2 Recent progress in ACQ based aPSs

In PDT, selective activation of PSs and precise signal regulation are essential for maximizing therapeutic efficacy while minimizing off-target damage. Conventional "always-on" fluorescent PSs often cause phototoxicity in normal tissues, whereas nanoparticle-based PSs exploiting ACQ offer a practical solution for controlled activation. In these systems, self-assembly or aggregation strongly suppresses fluorescence and ROS generation, maintaining the PS in an "off" state during circulation or in healthy tissues. Within the TME, local acidity (pH ∼6.5) or lysosomal pH (4.5–5.0) can disrupt the aggregates, abolishing ACQ and specifically restoring fluorescence and photodynamic activity. Consequently, pH responsiveness has emerged as a key design principle for ACQ-type aPSs, enabling tumor-specific

© 2026 The Author(s). Published by the Royal Society of Chemistry

Open Access Article. Published on 29 January 2026. Downloaded on 5/27/2026 1:04:59 AM.
This article is licensed under a Creative Commons Attribution-NonCommercial 3.0 Unported Licence.

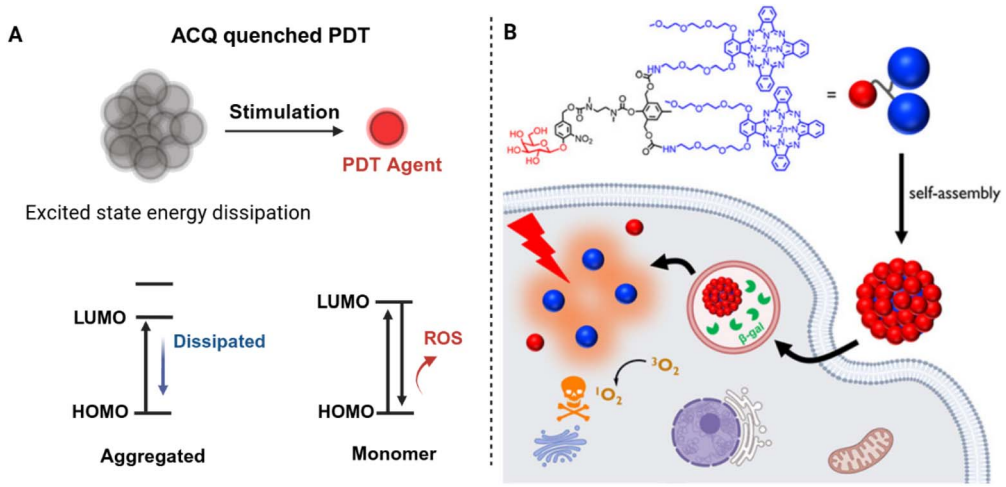

Fig. 11 Basic principle (A) and example (B) of ACQ based aPS design. Reproduced with permission from ref. 112. Copyright 2024, American Chemical Society.

imaging and providing a molecular basis for Type I PDT under hypoxic conditions.

Building on pH-responsive ACQ strategies, Song *et al.* developed dynamic nanoparticles BNP@R for combined ferroptosis and PDT.[116] Using PEG-*b*-PDPA as a carrier, acid-sensitive PBE bonds stably encapsulated the GSH peroxidase 4 (GPX4) inhibitor RSL-3, while conjugating the PS PPa. At neutral pH (7.4), BNP@R remained stable and inactive; upon exposure to acidic tumor endosomes/lysosomes (pH 5.8–6.2), the nanoparticles disassembled, releasing RSL-3 and restoring PPa fluorescence and photodynamic activity (Fig. 12A). *In vitro*, BNP@R plus 671 nm laser irradiation generated ROS, induced ICD, and synergized with RSL-3 to enhance lipid ROS accumulation and tumor cell apoptosis, while promoting bone marrow-derived dendritic cell maturation. *In vivo*, BNP@R accumulated in tumors *via* the EPR effect; laser treatment inhibited GPX4 and triggered ferroptosis. Combined with αPD-L1, it increased $CD8^+$ T cell infiltration and IFN-γ secretion, preventing tumor recurrence. In the 4T1 model, this approach reduced lung metastasis, achieved 35% tumor-free survival in 50 days, eliminated cancer stem cells, and maintained excellent biocompatibility.

Also based on pH response, Liu and her team addressed the key limitations of fluorescence-image-guided PDT, including background fluorescence interference, phototoxicity during circulation, and limited tumor penetration.[120] They designed an intelligent nanoplatform, LipoHPM, using a NIR PS MBA (a BDP derivative, $\lambda_{abs} = 630$ nm and $\lambda_{em} = 670$ nm) as the core. MBA was linked to biotin-PEG *via* an acid-labile amine linker to form photodynamic molecular (PM) micelles, which exhibited an ACQ-induced "OFF" state of fluorescence and ROS due to π–π stacking. These PM micelles, co-encapsulated with the tumor penetration enhancer HDZ, were incorporated into pH-sensitive liposomes (with biotin modification for active targeting). During blood circulation, LipoHPM remained stable and leakage-free. After tumor accumulation and endocytosis, the acidic lysosomal environment triggered liposome disassembly and PM micelle protonation/de-aggregation (de-ACQ), restoring strong NIR fluorescence (130-fold enhancement) and dual-type ROS generation ($^{\bullet}OH$ *via* type I and $^1O_2$ *via* type II). HDZ further improved tumor penetration by arresting cells in the G_0/G_1 phase and disrupting tight junctions, extending penetration depth from 100 μm to 500 μm. *In vitro*, LipoHPM exhibited uniform particle size (193.7 ± 21.4 nm), good serum stability, and strong phototoxicity toward 4T1 cells ($IC_{50} = 2.2$ μM under irradiation). *In vivo*, in 4T1 tumor-bearing mice, the tumor signal-to-background ratio reached 58 at 12 h post-injection. Upon light irradiation, tumor volume decreased to 35 mm^3 within 30 days without recurrence, and lung metastasis was

Table 4 ACQ based aPS design

Response factors	Range of stimulation	Response moiety	Photosensitizer	Fluorescence activation	ROS activation	Ref.
—	—	CB [8]	Toluidine blue	—	×2.5	113
GSH/pH	10 mM	Aryl chloride	BODIPY	—	×10	114
pH	pH 6.5–7.4	Schiff base bond	Pyrochlorophyll a	—	—	115
pH	pH 5.8–6.2	Phenylboronate ester bond	Pheophorbide a	×12		116
GSH	0–10 mM	Disulfide bond	MB	×17.7	—	117
pH	pH 5.0–7.4	Protonation of the tertiary amine group	TPP	×2.9	×∼6.1	118
GSH	0–10 mM	Disulfide bond	—	—	—	119
β-gal	1.5 U/mL	Glycosidic linkage	ZnPc	×4	—	112
pH	pH 5.0–5.5	Amino linker	Hemicyanine	×12.8	×32.4	120

Open Access Article. Published on 29 January 2026. Downloaded on 5/27/2026 1:04:59 AM.
This article is licensed under a Creative Commons Attribution-NonCommercial 3.0 Unported Licence.

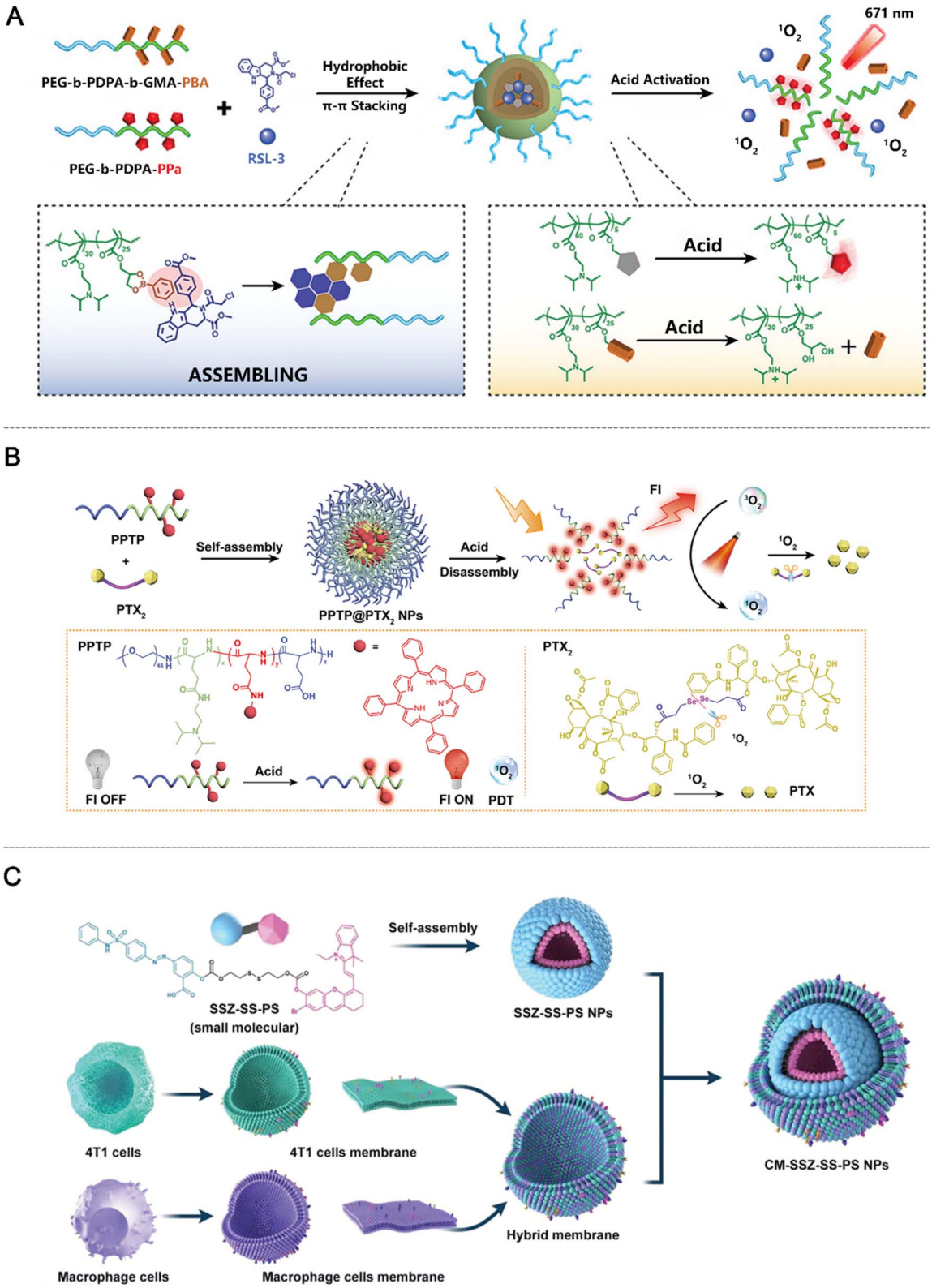

Fig. 12 Examples of ACQ based aPS design. (A) pH responsive ACQ nanoaPS design. Reproduced with permission from ref. 116. Copyright 2021, Wiley-VCH GmbH. (B) pH responsive ACQ nanoaPS design and the drug delivery system. Reproduced with permission from ref. 118. Copyright 2022, American Chemical Society. (C) GSH responsive self-assembled nano-prodrugs designed with the ACQ aPS. Reproduced with permission from ref. 121. Copyright 2024, Wiley-VCH GmbH.

© 2026 The Author(s). Published by the Royal Society of Chemistry

Open Access Article. Published on 29 January 2026. Downloaded on 5/27/2026 1:04:59 AM.
This article is licensed under a Creative Commons Attribution-NonCommercial 3.0 Unported Licence.

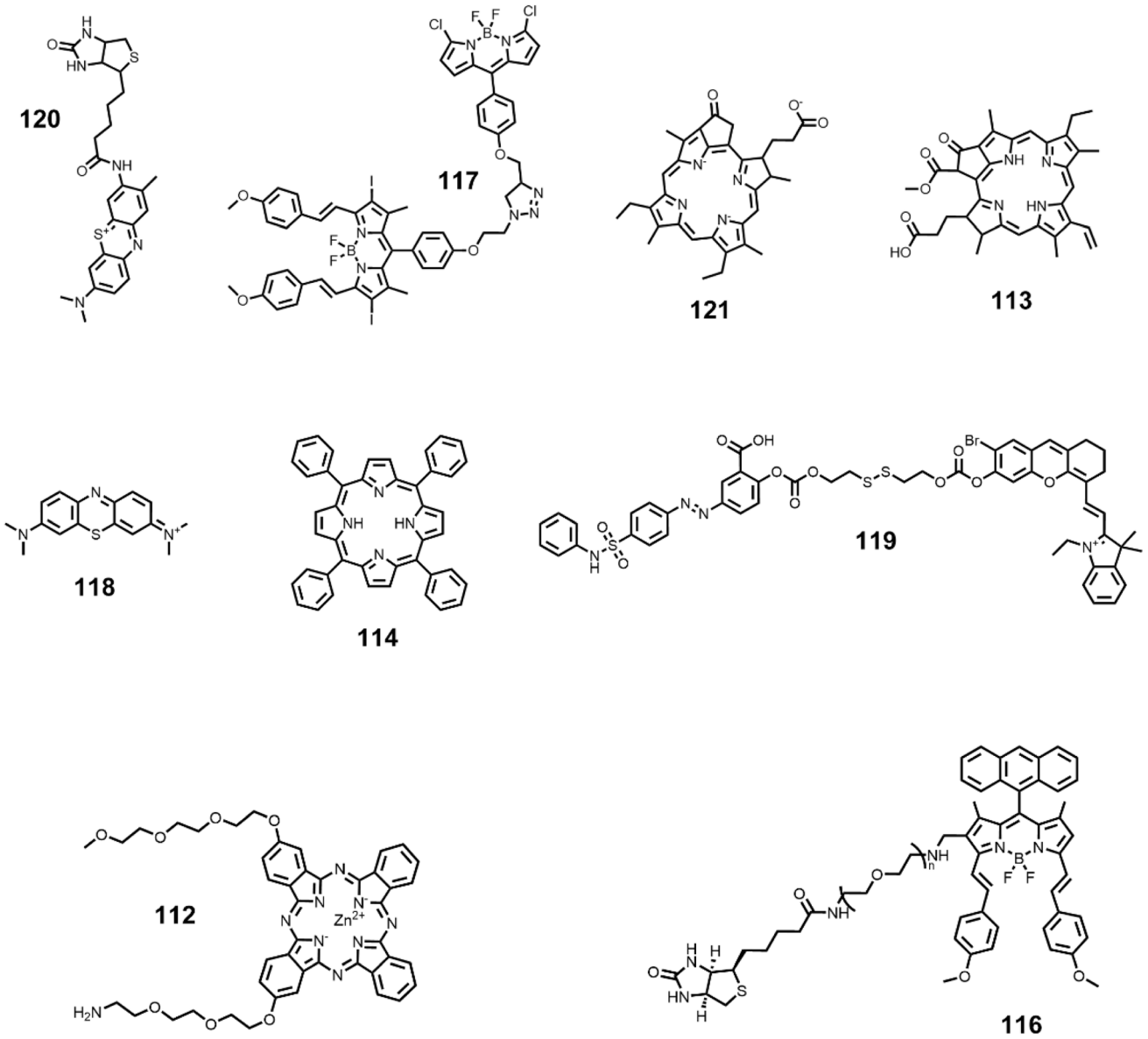

Fig. 13 The main structures of ACQ-based aPSs.

markedly suppressed, with no pathological damage to major organs. This study, building upon the pH-responsive ACQ strategy, achieved significant advancements by integrating NIR fluorescence optimization, HDZ-mediated penetration enhancement, and dual-mode ROS generation, thereby expanding the application of ACQ-based nanoplatforms in FIG-PDT and offering a promising strategy for precise solid tumor therapy.

Beyond single-mechanism ACQ designs, aPSs combining ACQ with additional activation strategies have shown great promise for precise tumor targeting. Zhang *et al.* developed dual-responsive biodegradable polypeptide nanoparticles, PPTP@PTX_2 NPs, for synergistic photodynamic–chemotherapy of breast cancer.[118] The system integrated an acid-sensitive group with a PS, enabling pH-triggered fluorescence and ROS generation in the acidic TME (Fig. 12B). The ROS further promoted drug release, achieving enhanced therapeutic effects. Both *in vitro* and *in vivo* studies demonstrated efficient tumor inhibition with minimal systemic toxicity, highlighting a versatile strategy for precise cancer treatment. Similarly, Teng *et al.* proposed a "dual-lock-and-key" design combining ACQ and FRET to construct supramolecular PSs, BIBCl-PAE NPs, overcoming traditional ACQ limitations and nonspecific phototoxicity.[114] The dual-BODIPY core included an iodine-substituted BI unit to enhance ISC and singlet oxygen generation and a chlorine-substituted BCl unit providing GSH responsiveness and energy-donor function, all encapsulated within a pH-responsive PEG-PAE copolymer. BIBCl-PAE NPs displayed uniform spherical morphology (85 ± 11 nm), a zeta potential of -8 ± 9 mV, excellent colloidal stability over 15 days in PBS, and high photostability in 10% FBS or under 48 h of white-light exposure. At neutral pH (7.4), ACQ and PEG-PAE micelle

Open Access Article. Published on 29 January 2026. Downloaded on 5/27/2026 1:04:59 AM. This article is licensed under a Creative Commons Attribution-NonCommercial 3.0 Unported Licence.

encapsulation kept the PS inactive. Under acidic tumor-like conditions (pH 5.0–6.8) with high GSH (1–15 mM), PEG-PAE protonation triggered micelle disassembly and BIBCl release. GSH substitution of the chlorine on the BCl unit formed water-soluble BIBSG, where FRET between BGS and BI units (64% efficiency) enhanced $^1O_2$ generation by 10-fold relative to the inactive state and 2-fold relative to Ce6. Biologically, BIBCl-PAE NPs were selectively activated in HepG2, A549, and HeLa cells, showing a 7-fold NIR fluorescence increase and light-triggered cytotoxicity (IC_{50} = 4.5–5.2 μg mL^{-1}) while maintaining >85% viability in normal LO2 cells. *In vivo*, tumor fluorescence peaked at 9 h post-intravenous injection in HepG2 xenografts, and light irradiation over 14 days resulted in significant tumor suppression, including complete regression in 2 mice, without histopathological organ damage, weight loss, or systemic toxicity.

Building on GSH-responsive ACQ strategies, Zeng *et al.* designed a single-molecule self-assembled nanoprodrug (MSSP-NP) to overcome GSH-mediated tumor drug resistance and achieve synergistic photodynamic–chemotherapy.[117] The MSSP molecule linked methylene blue (MB) and a GSH-sensitive Pt(IV) prodrug *via* a disulfide bridge, with a tumor-targeting CPA-PAPRGD peptide for enhanced selectivity. In its inactive state, the disulfide linkage quenched MB photoactivity and MSSP self-assembled into stable ~100 nm nanoparticles that accumulated in tumors through EPR and RGD-mediated targeting. In the high-GSH TME, disulfide cleavage released MB, Pt (IV), and quinone methide, cooperatively depleting ~80% of intracellular GSH. Upon 680 nm laser irradiation, MB generated $^1O_2$ for PDT, while Pt(IV) reduced to Pt(II) exerted chemotherapeutic effects. *In vitro*, the combined treatment killed 80% of A549cis cells at 20 μM with irradiation, outperforming free Pt(IV) (20%). *In vivo*, tumor fluorescence and photoacoustic signals peaked at 8 h post-injection, and 18-day laser treatment resulted in 96.4% tumor inhibition without systemic toxicity.

Expanding this concept, Li *et al.* developed a GSH-activated single-molecule self-assembled nanoprodrug (SSZ-SS-PS) with hybrid membrane coating to tackle intrinsic ROS resistance in triple-negative breast cancer.[119] Amphiphilic SSZ-SS-PS linked a cyanine-derived PS (λ_{abs} = 666 nm; λ_{em} = 721 nm) and the SLC7A11 inhibitor sulfasalazine (SSZ) *via* a GSH-responsive disulfide bond, driving self-assembly into ~50 nm nanospheres (PDI of 0.08–0.15) with 30-day colloidal stability (Fig. 12C). Under physiological conditions, ICT kept the PS and SSZ inactive, minimizing off-target toxicity. In triple-negative breast cancer, 1–15 mM GSH cleaved the disulfide bond, releasing the PS and SSZ; light irradiation (40 mW cm^{-2}) triggered the PS to generate $^1O_2$ and restore NIR fluorescence, while SSZ inhibited cystine uptake and GPX4 activity, depleting >60% of GSH to overcome ROS resistance. Coating with hybrid 4T1/RAW 264.7 cell membranes (CM-SSZ-SS-PS NPs, 231.2 nm, zeta −8.9 mV) preserved membrane proteins, enhancing serum stability and tumor uptake (1.8-fold) while reducing normal cell toxicity (viability >85%). *In vitro*, optimal PS : SSZ (1 : 1) ratios achieved 2.3-fold higher apoptosis than the free PS with elevated ROS. *In vivo*, tumor fluorescence peaked at 6 h (3.5× higher than that of uncoated), shrinking tumors to ~100 mm^3 *versus* >700 mm^3 for the free PS within 21 days, reducing lung metastases (<5 nodules/mouse *vs.* >30), and extending survival (>60 days in 4/5 mice) without organ damage. Western blot confirmed SLC7A11 and GPX4 downregulation (−55% and −48%, respectively). Together, these studies establish a translatable paradigm for GSH-activated, ROS-resistance-suppressing, and tumor-targeted PDT with synergistic chemo-photodynamic effects.

In conclusion, ACQ, traditionally viewed as a limitation of conventional PSs, has been strategically exploited in the design of aPSs to address the central challenge of balancing off-target phototoxicity with tumor-specific activation in PDT. By leveraging the ACQ effect, aPSs remain in an "OFF" state during circulation, with aggregation suppressing both fluorescence and ROS generation, thereby protecting normal tissues. Upon exposure to tumor-specific stimuli—such as acidic pH or elevated GSH levels—these aPSs undergo disassembly (de-ACQ), restoring photoreactivity and fluorescence and enabling precise "circulation-silent, tumor-active" control. Experimental studies have demonstrated that ACQ-based designs have evolved from single-stimulus responsiveness to multi-mechanistic synergy, including coupling with PET to stabilize the OFF state, integrating FRET to enhance ROS generation, and incorporating GSH responsiveness to overcome ROS resistance. Delivery performance has been further optimized *via* single-molecule self-assembly and biomimetic membrane coatings. Overall, ACQ not only addresses the challenge of targeted aPS activation but also functions as a central design node linking stimulus responsiveness, functional integration, and therapeutic enhancement, providing a key paradigm for the clinical translation of PDT.

6 AIE-based design of aPSs

6.1 Design principles and basic mechanisms

AIE is a proximity-dependent mechanism frequently used in aPSs.[122–124] AIE-active molecules usually contain large, flexible, and hydrophobic π-conjugated structures.[125,126] In a monomeric or well-dispersed state, intramolecular motions such as rotation and vibration consume excitation energy through non-radiative relaxation. As a result, both fluorescence and ROS generation are weak. When the molecules aggregate, these internal motions are restricted. Energy is then released through radiative emission or intersystem crossing, which leads to strong fluorescence and efficient ROS production.[127] This process forms the basis of AIE-based activation.

In typical designs, AIE-based aPSs remain inactive in solutions or in normal tissues. Aggregation is triggered by disease-related signals such as enzymatic cleavage, pH change, altered viscosity, or polarity variation in the TME. Once aggregation occurs, both fluorescence and photodynamic effects are turned on. The AIE mechanism allows precise control of where and when activation happens. By adjusting molecular hydrophobicity, rigidity, and aggregation tendency, researchers can fine-tune the responsiveness and selectivity of the system (Fig. 14A). For example, in the study published by Xiong *et al.* in 2024, the authors designed an ALP-responsive AIE probe, TPE-APP (Fig. 14B). TPE-APP is functionalized with phosphate groups, giving it good solubility and keeping it monodispersed under

© 2026 The Author(s). Published by the Royal Society of Chemistry

Open Access Article. Published on 29 January 2026. Downloaded on 5/27/2026 1:04:59 AM. This article is licensed under a Creative Commons Attribution-NonCommercial 3.0 Unported Licence.

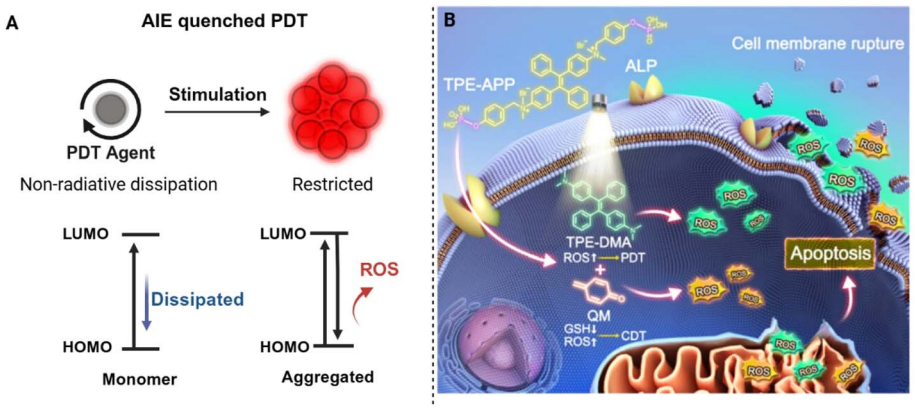

Fig. 14 Basic principle (A) and example (B) of AIE based aPS design. Reproduced with permission from ref. 128. Copyright 2024, American Chemical Society.

physiological conditions, where it exhibits weak fluorescence and minimal ROS generation due to free intramolecular rotation of the TPE core.[128] When encountering ALP, overexpressed in prostate, breast, and bone cancers, enzymatic dephosphorylation triggers aggregation of the hydrolysis product TPE-DMA, activating strong yellow-green fluorescence (400-fold increase) for tumor imaging and generating quinone methide intermediates. The aggregates produce $^1O_2$ under white light for PDT, while QM intermediates enable oxygen-independent CDT by generating ROS and depleting intracellular GSH (~40% in HeLa cells), amplifying oxidative stress synergistically. *In vitro*, TPE-APP selectively lights up ALP-high cancer cells (HeLa, HepG2, RD) within 5 minutes, disrupts membranes and mitochondrial potential within 30 minutes, and reduces viability to ~9% at 10 μM under light, while ALP-low normal MDCK cells remain >90% viable. Subcellular localization shows predominant membrane accumulation (Pearson correlation coefficient up to 88.3%) with minor mitochondrial targeting, promoting apoptosis. *In vivo*, intratumoral injection in HeLa xenograft mice produces immediate fluorescence activation (peak at 1 minute), which is blocked by the ALP inhibitor sodium orthovanadate, and combinatorial CDT-PDT treatment inhibits tumor growth by 84.5% over 14 days without significant weight loss, hematological changes, or organ toxicity. This work advances the enzyme-instructed self-assembly (EISA)-based AIE aPS design by combining dual therapeutic modalities, biomarker-responsive imaging, and hypoxia-resistant therapy, while maintaining biocompatibility and safety. TPE-APP provides a versatile template for modern AIE probes for precise cancer theranostics. Compared with other activation modes, AIE offers several advantages, including a high signal-to-background ratio, stability against self-quenching, and amplified ROS output at the target site. These characteristics make AIE-based PSs an appealing platform for selective, efficient, and low-toxicity PDT (Table 5 and Fig. 16).

6.2 Recent progress in AIE-based aPSs

As a pioneering study on AIE-based aPSs, Liu and her team in 2015 first integrated AIE characteristics with enzyme-responsive activation mechanisms, overcoming the intrinsic limitations of traditional ACQ PSs and establishing a novel paradigm for aPS design.[129] The core concept involved synthesizing enzyme-responsive AIE PSs by using tetraphenylethylene (TPE) as the AIE-active core and linking hydrophilic segments *via* enzyme-cleavable peptide bonds to construct amphiphilic "hydrophilic–hydrophobic" molecules (Fig. 15A). In aqueous solution, the hydrophilic segment maintained the molecule in a dispersed state, allowing free intramolecular motion of the TPE unit, thereby suppressing both fluorescence and singlet oxygen generation ("OFF" state) and minimizing background

Table 5 AIE based aPS design

Response factors	Range of stimulation	Response moiety	Photosensitizer	Fluorescence activation	ROS activation	Ref.
CTSB	10 μg mL^{-1}	Peptide	TPP	—	—	129
ALP	0–1 U mL^{-1}	FpYGpYGpY	TPE	—	—	130
GSH	0.5–10 mM	—	TPAAQ	—	—	131
H_2O_2	0–100 μM	Boronate ester	Tetraphenylpyrazine	×~24	—	132
H_2O_2	0–100 μM	Boronate ester	TPA	—	—	133
ALP	0–100 U L^{-1}	Phosphate group	TPA	×50	—	134
Hypoxia	0–10 μg mL^{-1}	Arylazo	TPFN	×~54	—	135
Hypoxia	0–10 μg mL^{-1}	Azobenzene linker	AIEgen T-2TM	×7	×1.8	85
ALP	0–160 U L^{-1}	Phosphate group	TPE	—	—	128
GSH/Cys	0–10 mM	F_4TCNQ	TPA	—	—	63

Open Access Article. Published on 29 January 2026. Downloaded on 5/27/2026 1:04:59 AM.
This article is licensed under a Creative Commons Attribution-NonCommercial 3.0 Unported Licence.

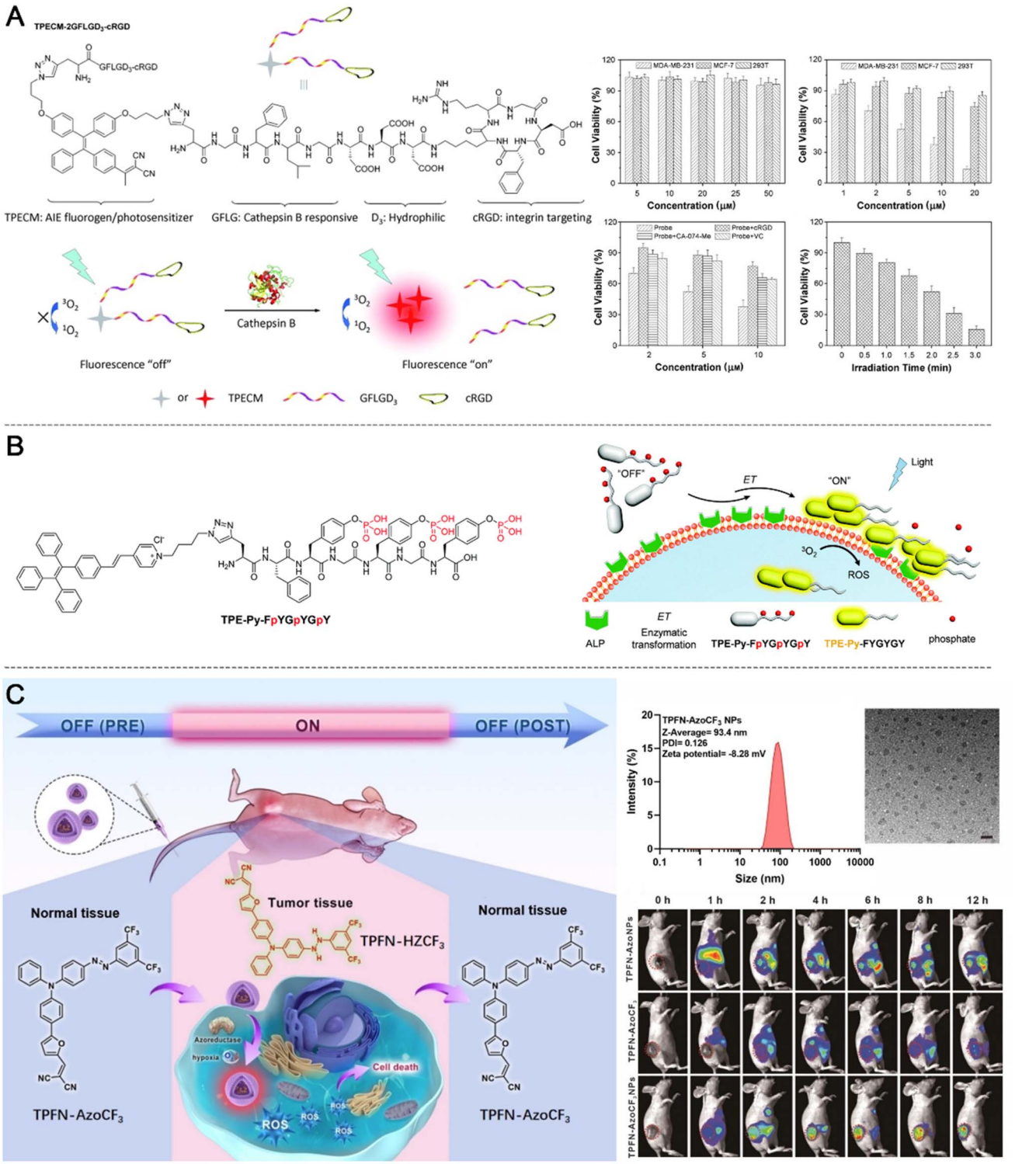

Fig. 15 Examples of AIE based aPS design. (A) CTSB responsive AIE nanoaPS design. Reproduced with permission from ref. 129. Copyright 2015, Wiley-VCH GmbH. (B) Enzyme-instructed self-assembly aPS design. Reproduced with permission from ref. 130. Copyright 2018, The Royal Society of Chemistry. (C) Hypoxia responsive AIE aPS design. Reproduced with permission from ref. 135. Copyright 2024, Wiley-VCH GmbH.

toxicity. Upon entering TMEs containing specific hydrolytic enzymes, the peptide bonds were selectively cleaved, releasing the hydrophilic segments. The remaining hydrophobic TPE units rapidly aggregated, restricting intramolecular motion, triggering the AIE effect, and simultaneously restoring strong fluorescence and efficient $^1O_2$ generation ("ON" state), achieving integrated "enzyme activation-imaging-PDT." This work was the first to demonstrate that AIE can serve as a precise activation switch for aPSs, coupling enzyme specificity with aggregation-induced activation, thereby addressing the dual

© 2026 The Author(s). Published by the Royal Society of Chemistry

Open Access Article. Published on 29 January 2026. Downloaded on 5/27/2026 1:04:59 AM.
This article is licensed under a Creative Commons Attribution-NonCommercial 3.0 Unported Licence.

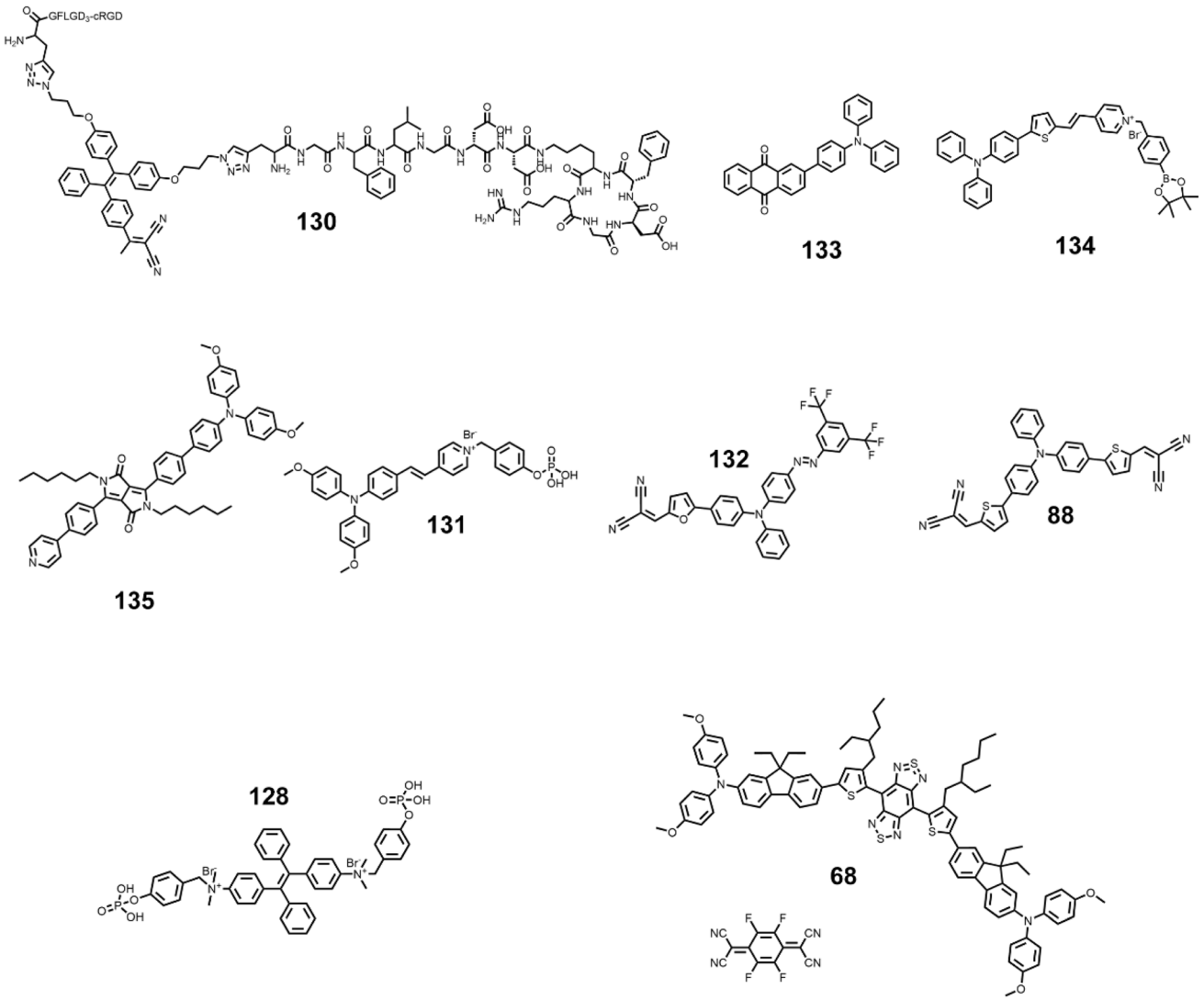

Fig. 16 The main structures of AIE-based aPSs.

challenges of "aggregation-caused quenching" and "nonspecific activation" inherent to traditional PSs. It represents the foundational work in the AIE-based aPS field.

In 2018, Ji and colleagues further advanced the design of enzyme-responsive AIE-based aPSs by deeply integrating EISA with AIE properties, achieving precise fluorescence imaging and PDT of cancer cells with high alkaline phosphatase (ALP) expression.[130] Building on the "aggregation-activated" principle established in 2015, this study innovatively incorporated EISA into the activation mechanism, using enzyme-catalyzed self-assembly to enhance both the efficiency of AIE triggering and targeting specificity (Fig. 15B). By selecting ALP, a widely expressed tumor marker, as the target, the work expanded the applicability of AIE aPSs and provided a critical reference for subsequent molecular design and clinical translation of enzyme-responsive AIE aPSs. It represents a key step in the field, moving from concept validation toward optimized targeting strategies. Building on the pioneering work of Ji *et al.*, subsequent studies have further enhanced the diagnostic–therapeutic contrast and application depth of ALP-responsive aPSs by introducing chromophores with long-wavelength emission potential and more efficient shielding strategies. In 2023, Lam *et al.* reported a phosphate-modified probe, TPAPY-PO, based on a near-infrared AIE core (TPAPY).[134] In this design, the phosphate group confers good water solubility, allowing the probe to remain in a monodispersed state under physiological conditions, where intramolecular motion dissipates the excited-state energy and both fluorescence and photodynamic activity remain in an "OFF" state. Upon encountering ALP-overexpressing cancer cells, the phosphate group is specifically hydrolyzed, and the resulting hydrophobic TPAPY core rapidly aggregates to trigger the AIE effect. This *in situ* aggregation process not only activates intense near-infrared fluorescence for high-contrast tumor imaging but also markedly enhances singlet oxygen generation, enabling precise eradication of tumor cells. By integrating the deep-tissue penetration advantage of near-infrared imaging with the precise control afforded by enzyme-mediated assembly, these studies indicate

Open Access Article. Published on 29 January 2026. Downloaded on 5/27/2026 1:04:59 AM. This article is licensed under a Creative Commons Attribution-NonCommercial 3.0 Unported Licence.

that ALP-responsive aPSs are evolving toward higher spatiotemporal resolution and greater clinical translation potential.

Liu's team further advanced AIE-based aPS design by combining the delivery advantages of metal–organic frameworks (MOFs) with the optical properties of AIE PSs.[131] They constructed rod-shaped mesoporous Cu-MOFs *via* defect engineering to overcome the limitations of traditional MOF carriers, such as low drug loading, poor tumor targeting, and activity suppression of AIE PSs during delivery, providing a new strategy for PDT carrier design. Mechanistically, the platform enables precise control through a "carrier protection → tumor response → activity restoration" sequence. Under normal physiological conditions, the Cu-MOF channels isolate TPAAQ from oxygen, maintaining the PS in an "OFF" state ($^1O_2$ generation <10%). Upon entering tumor cells, high intracellular GSH concentrations (0.5–10 mM) reduce Cu^{2+}, triggering MOF disassembly and TPAAQ release, while Cu^{2+} consumption of GSH (~50 μg per mL MOF removes 0.5 mM GSH) alleviates ROS scavenging. Released TPAAQ aggregates to activate AIE, restoring strong far-red fluorescence (emission peak at 680 nm) for imaging and efficiently generating $^1O_2$ under white light (100 mW cm^{-2}) with 9,10-anthracenediyl-bis(methylene)dimalonic acid degradation >80%, enabling activatable PDT. In HeLa xenograft mice, the rod-shaped nanorods achieved peak tumor accumulation fluorescence at 12 h, 1.8-fold higher than that of nanodots (NDs) at 8 h, with enhanced tumor penetration (deep tissue fluorescence is 3.5-fold higher than that of NDs). Combined with light irradiation, tumor inhibition reached 85%, compared to 52% for the ND group, with no pathological damage to major organs, confirming good biosafety. This study represents the first integration of rod-shaped mesoporous MOFs with AIE PSs, employing defect engineering and morphology control to simultaneously enhance MOF drug loading, targeted delivery, and AIE PS activity modulation, establishing a paradigm for MOF-based AIE PS delivery systems and advancing PDT carriers toward "high loading → precise targeting → controllable activation".

Building on the general design principles of AIE-based aPSs, recent studies have demonstrated the versatility of this strategy for TME-responsive PDT. For instance, Wu *et al.* developed a H_2O_2-responsive AIE probe, TTPy-H_2O_2, which utilizes a boronate ester moiety for specific recognition and a pyridinium cation for initial mitochondrial targeting.[132] Upon responding to H_2O_2, the probe undergoes a conversion that shifts its localization from mitochondria to lipid droplets, accompanied by a distinct change from red/NIR to yellow fluorescence. This dual-signal read-out enables real-time monitoring of mitochondrial damage during PDT, providing a powerful tool for investigating ROS-induced cellular responses.

Similarly, Li *et al.* reported a H_2O_2-responsive small-molecule AIE-based aPS, DPP-BPYS, as a representative example.[133] This PS features a DPP core functionalized with a boronate ester moiety, enabling selective responsiveness to elevated H_2O_2 levels in tumor tissues. Under physiological conditions, DPP-BPYS remains in a dispersed, non-aggregated state, with fluorescence and photodynamic activity effectively "off". In the presence of tumor-associated H_2O_2, oxidation of the boronate ester converts DPP-BPYS into hydrophobic DPP-BPY, inducing aggregation and triggering the AIE effect. This transition restores NIR fluorescence (684 nm and a Stokes shift of 180 nm) and efficient singlet oxygen generation. Notably, DPP-BPY demonstrates selective subcellular targeting, preferentially accumulating in lipid droplets ($C\log P = 14.284$) with a high co-localization coefficient of 0.96 relative to commercial lipid droplet probes. *In vitro*, H_2O_2-triggered activation combined with white light irradiation effectively kills tumor cells (MCF-7 and ZJU0430) and induces apoptosis *via* Bax upregulation and Caspase-3 activation. *In vivo*, in an inflammation mouse model, DPP-BPYS enables specific imaging of endogenous H_2O_2, exhibiting an 8.2-fold fluorescence enhancement in 45 minutes, with no detectable toxicity to major organs. This work exemplifies a concise and efficient molecular paradigm for designing small-molecule, TME-responsive AIE-based aPSs, integrating precise stimulus-triggered activation, subcellular targeting, and high photodynamic efficiency.

Similarly, based on TME responsiveness, in 2023, a study reported the design of a hypoxia-normoxia reversible I-type AIE-based aPS, TPFN-AzoCF$_3$, addressing limitations of traditional PDT such as pre- and post-treatment phototoxicity and low efficacy under tumor hypoxia.[135] The PS combines a triphenylamine-derived I-type AIE core (TPFN, producing ROS under low oxygen) with a trifluoromethyl-substituted azobenzene group (AzoCF$_3$) as a hypoxia-responsive switch (Fig. 15C). Under normoxic conditions, the EZ isomerization of AzoCF$_3$ consumes TPFN's excited-state energy, keeping fluorescence and ROS generation "OFF." In hypoxic tumor environments, the azobenzene is reduced to a hydrazine derivative (TPFN-HZCF$_3$), triggering AIE, restoring NIR fluorescence (671 nm), and producing I-type ROS (mainly hydroxyl radicals). This process is reversible, allowing the PS to return to the "OFF" state in normoxia, thus minimizing phototoxicity outside tumors. *In vitro*, TPFN-AzoCF$_3$ exhibited a 54-fold fluorescence increase under 0.1% oxygen, with an IC_{50} of 5.686 μM in HeLa cells and negligible toxicity to normal HEK293 cells (IC_{50} > 50 μM). *In vivo*, DSPE-PEG-2000-coated nanoparticles (~100 nm) accumulated in HeLa xenograft tumors *via* the EPR effect, showing strong tumor fluorescence within 60 minutes. Combined light treatment over 21 days significantly inhibited tumor growth, with no skin phototoxicity or organ damage. This study provides a new paradigm for designing hypoxia-responsive AIE-based aPSs for precise and safe PDT in the TME. Expanding on this logic, the coupling of hypoxia-responsive AIE systems with advanced therapeutic outcomes, such as pyroptosis-mediated immunotherapy, has further broadened the clinical potential of these agents. Recent designs have demonstrated that hypoxia-triggered AIE activation can serve as a potent inducer of immunogenic cell death, effectively transforming local photodynamic damage into a systemic anti-tumor immune response.[85] Despite the success of hypoxia-targeted strategies, the tumor microenvironment is also characterized by other distinct biochemical hallmarks that can be leveraged for even greater precision. Chief among these is the significant redox gradient maintained by intracellular GSH, which has inspired

© 2026 The Author(s). Published by the Royal Society of Chemistry

Open Access Article. Published on 29 January 2026. Downloaded on 5/27/2026 1:04:59 AM. This article is licensed under a Creative Commons Attribution-NonCommercial 3.0 Unported Licence.

the development of a diverse array of GSH-responsive AIE photosensitizers designed for specific intracellular activation.

Wu *et al.* developed bovine serum albumin-encapsulated activatable NIR AIE PS nanoparticles (a-NA-PSNPs), integrating a NIR AIE PS (N-PS) with a cysteine (Cys)/GSH-responsive charge transfer complex (CTC).[63] Under physiological conditions, the CTC serves as an energy acceptor, quenching both N-PS NIR-II fluorescence and ROS generation. Upon exposure to the TME, elevated Cys/GSH levels degrade the CTC, restoring N-PS fluorescence and photodynamic activity. *In vitro*, a-NA-PSNPs selectively killed 4T1 and other cancer cells while exhibiting minimal toxicity to normal cells, and *in vivo* studies in 4T1 tumor-bearing mice demonstrated high signal-to-background NIR-II imaging-guided PDT with significant tumor suppression and excellent biocompatibility. This study exemplifies current trends in AIE aPS development: moving from single-enzyme-triggered activation to multi-mechanism cooperative regulation, here, combining FRET-mediated quenching with AIE activation to enhance selectivity. It highlights adaptation to complex TMEs, integrating redox modulation with Cys/GSH responsiveness to maximize therapeutic efficacy. Furthermore, the design emphasizes theranostic integration, achieving precise coordination of NIR-II imaging and PDT, while BSA encapsulation improves biocompatibility and *in vivo* stability. Collectively, these advances illustrate the evolution of AIE aPS platforms toward precise, microenvironment-responsive cancer therapy with clinical translatability.

AIE-based aPSs provide a robust and highly versatile platform for achieving precise control over both fluorescence emission and ROS generation. By exploiting aggregation-induced restriction of intramolecular motions, AIE enables stimulus-responsive activation in response to a variety of pathological cues, including enzymatic cleavage, pH changes, oxidative stress, or local viscosity shifts. Rational tuning of molecular hydrophobicity, conjugation, and flexibility allows precise modulation of aggregation behavior, activation kinetics, and photodynamic output, while minimizing background fluorescence and off-target phototoxicity. Furthermore, AIE-based aPSs can be integrated with subcellular targeting strategies or multifunctional delivery systems, enabling imaging-guided PDT with high spatial specificity. Collectively, these features establish AIE as a powerful design principle for next-generation aPSs, offering controllable, selective, and clinically translatable tumor-targeted PDT.

7 Conclusions and future prospects

APSs have emerged as a pivotal advancement in PDT, fundamentally addressing the longstanding limitation of nonspecific phototoxicity that constrains conventional "always-on" PSs.[136,137] Through mechanism-guided molecular design, aPSs achieved precise spatiotemporal control over their photodynamic activity. They remain inert under normal physiological conditions and activate exclusively in response to tumor-specific stimuli within the TME, thereby aligning PDT with the core objectives of precision medicine. This review has systematically explored five core design strategies for effective aPS, all leveraging distinct photophysical or photochemical mechanisms to regulate the "on–off" switch of photoreactivity while integrating diagnostic capabilities, which collectively enhance treatment safety and efficacy.

These design strategies converge on modulating aPS activity *via* TME cues, though each follows unique regulatory logic. Some rely on adjusting energy transfer between PS donors and quenchers: in inactive states, efficient energy transfer suppresses fluorescence and reactive ROS generation, while TME stimuli disrupt this transfer to restore photoreactivity. Others regulate electron flow between the PS and quenching moieties, with TME factors like acidic pH or hypoxia-driven enzymatic reactions interrupting electron transfer to reactivate the system. Additional strategies focus on ICT or aggregation behavior: certain aPSs used "caging" groups to suppress charge redistribution, with tumor-overexpressed enzymes removing these groups to reactivate ROS production; others inverted traditional ACQ limitations, forming stable aggregates during circulation to keep activity "off" and relying on TME stimuli for disassembly and photoreactivity restoration; still others exploit AIE, where TME-triggered aggregation restricts intramolecular motion, simultaneously enhancing fluorescence imaging and ROS generation that are suppressed in monomeric states. Together, these designs have transformed PDT from a non-selective approach to a targeted therapy, minimizing healthy tissue damage while maximizing tumor-specific efficacy.

Despite significant progress in aPS development, several challenges remain to fully unlock their clinical potential. It is critical to enhance the adaptability to the complex TME, particularly for deep-seated and hypoxic tumors, as current aPSs often respond to visible or NIR-I light with limited tissue penetration;[138–140] advancing NIR-responsive designs or combining aPSs with materials that convert light to more penetrative wavelengths can address deep-tissue treatment needs, while optimizing Type I ROS generation pathways will improve efficacy in hypoxic regions where Type II ROS production is oxygen-constrained.

Improving the robustness of aPS activation in the heterogeneous TME is also essential, as single-stimulus responsive systems may fail to activate uniformly across tumors with variable stimulus distribution. Developing designs that respond to combinations of TME cues, such as pH paired with redox changes or enzyme activity paired with hypoxia, will enhance activation reliability, and integrating multiple quenching mechanisms into a single aPS system can further suppress background activity, reducing off-target phototoxicity risks.[25,141] Another key strategy to further enhance the robustness of aPSs lies in the development of intelligent systems that integrate multiple mechanisms in a synergistic manner. For example, Kocak *et al.* recently reported a dual-enzyme–responsive photosensitizer, RAM, based on an iodinated tryptanthrin core, in which APN and MAO are sequentially gated through an AND logic operation to achieve highly specific recognition of neuroblastoma cells.[142] This design markedly improves the safety profile of PDT by minimizing off-target activation. Nevertheless, future designs are expected to evolve toward even higher levels of intelligence, focusing on constructing multifunctional, self-

Open Access Article. Published on 29 January 2026. Downloaded on 5/27/2026 1:04:59 AM. This article is licensed under a Creative Commons Attribution-NonCommercial 3.0 Unported Licence.

regulating systems capable of addressing tumor heterogeneity and the complexity of the tumor microenvironment. The "dual-lock" activatable probe reported by Wei *et al.* provides a representative example in this direction.[143] This probe ingeniously employs GGT and NTR as two logical switches, enabling an automatic transition from a PDT mode at the tumor periphery to a PTT mode in the hypoxic tumor core. By dynamically coupling the recognition of multiple biomarkers with adaptive therapeutic modalities, this design strategy not only overcomes the intrinsic oxygen dependence of conventional aPSs but also offers a new paradigm for achieving full-process precise intervention. Such highly intelligent, self-adjustable aPS systems mark a critical shift from "passive responsiveness" toward "active adaptation to heterogeneity."

Advancing delivery systems is key to enhancing tumor accumulation and biocompatibility, as current carriers often face issues like rapid clearance by the reticuloendothelial system,[144] poor tumor penetration,[145,146] or potential immunogenicity.[147] Biomimetic carriers leveraging biological membrane properties can reduce clearance and improve biocompatibility, while active targeting strategies using tumor-specific ligands and environment-adaptive carriers that respond to TME cues for controlled release will further optimize aPS delivery to tumor parenchyma.[148,149]

Accelerating clinical translation requires addressing safety concerns and establishing standardized evaluation methods.[150] Long-term toxicity assessments of aPSs and their carriers, including evaluations of chronic organ damage, persistent phototoxicity, and metabolic profiles, are insufficient and need expansion to meet clinical standards. The lack of unified criteria for evaluating aPS performance, such as ROS generation efficiency, activation threshold, and imaging signal-to-background ratio, hinders cross-study comparisons; establishing consistent *in vitro* and *in vivo* evaluation protocols will facilitate screening of clinically viable candidates, and developing scalable synthesis methods will reduce production costs to support large-scale clinical applications.

Integrating emerging technologies will drive the development of more intelligent aPSs. Artificial intelligence can accelerate molecular design by predicting structure–activity relationships, optimizing properties like light responsiveness and stimulus specificity while reducing trial-and-error in synthesis. Real-time imaging technologies, such as photoacoustic imaging or fluorescence lifetime imaging, can be combined with aPSs to enable imaging-guided PDT, allowing real-time monitoring of aPS activation and tumor response to adjust treatment parameters for personalized therapy.[151] Self-monitoring aPSs, which exhibit activation-dependent fluorescence changes, can also provide direct feedback on therapeutic efficacy, further enhancing treatment precision.

In summary, aPSs have redefined PDT as a precision therapeutic approach, with diverse mechanism-guided designs enabling tumor-specific activation and integrated theranostic functions.[152] By addressing current challenges in TME adaptability, activation robustness, delivery efficiency, clinical translation, and technological integration, aPSs will continue to advance toward more personalized, effective, and safe cancer treatment. Their ongoing development and optimization will solidify their role as a cornerstone of precision oncology, expanding clinical impact across the treatment of diverse malignancies.

Author contributions

Kai Wang: conceptualization, investigation, writing – original draft (lead), review and editing. Xiaoying Mao: writing – original draft (supporting). Wuyan Xie: writing – original draft (supporting). Qin Zhou: review and editing. Xiaoyan Liu: review and editing. Dan Wu: conceptualization, review and editing. Qing Zhu: conceptualization, review and editing, supervision and funding acquisition. Bin Liu: conceptualization, review and editing, supervision and funding acquisition.

Conflicts of interest

There are no conflicts to declare.

Data availability

No primary research results, software or code have been included and no new data were generated or analyzed as part of this review.

Acknowledgements

This work was supported by the Tan Chin Tuan Centennial Professorship (E-467-00-0012-02), the National Research Foundation Investigatorship (A-8002259-00-00), the Zhejiang Provincial Medical and Health Technology Plan (2024KY1749) and the Traditional Chinese Medicine Science and Technology Research Project of Jinhua (2025ZD04).

Notes and references

1 J. D. Spikes, in *The Science of Photomedicine*, ed J. D. Regan and J. A. Parrish, Springer US, Boston, MA, 1982, pp. 113–144.
2 *Fluorescent Chemosensors*, ed. L. Wu, A. C. Sedgwick, X.-P. He and T. D. James, The Royal Society of Chemistry, 2023.
3 W. Jiang, M. Liang, Q. Lei, G. Li and S. Wu, The Current Status of Photodynamic Therapy in Cancer Treatment, *Cancers*, 2023, **15**, 585.
4 B. Ji, M. Wei and B. Yang, Recent advances in nanomedicines for photodynamic therapy (PDT)-driven cancer immunotherapy, *Theranostics*, 2022, **12**, 434–458.
5 J. M. Dąbrowski and L. G. Arnaut, Photodynamic therapy (PDT) of cancer: from local to systemic treatment, *Photochem. Photobiol. Sci.*, 2015, **14**, 1765–1780.
6 R. Alzeibak, T. A. Mishchenko, N. Y. Shilyagina, I. V. Balalaeva, M. V. Vedunova and D. V. Krysko, Targeting immunogenic cancer cell death by photodynamic therapy: past, present and future, *J. Immunother. Cancer*, 2021, **9**, e001926.
7 F. Du, Z. Chen, X. Li, X. Hong, L. Wang, F. Cai, N. Yang and C. Yu, Organelle-targeted photodynamic platforms: from

© 2026 The Author(s). Published by the Royal Society of Chemistry

Open Access Article. Published on 29 January 2026. Downloaded on 5/27/2026 1:04:59 AM. This article is licensed under a Creative Commons Attribution-NonCommercial 3.0 Unported Licence.

ICD activation to tumor ablation, *Chem. Commun.*, 2025, **61**, 12835–12847.
8 P. Liang, B. Ballou, X. Lv, W. Si, M. P. Bruchez, W. Huang and X. Dong, Monotherapy and Combination Therapy Using Anti-Angiogenic Nanoagents to Fight Cancer, *Adv. Mater.*, 2021, **33**, e2005155.
9 R. Bhuvaneswari, Y. Y. Gan, K. C. Soo and M. Olivo, The effect of photodynamic therapy on tumor angiogenesis, *Cell. Mol. Life Sci.*, 2009, **66**, 2275–2283.
10 Q. Yu, X. Li, J. Wang, L. Guo, L. Huang and W. Gao, Recent Advances in Reprogramming Strategy of Tumor Microenvironment for Rejuvenating Photosensitizers-Mediated Photodynamic Therapy, *Small*, 2024, **20**, e2305708.
11 Z. Yang, Y. Luo, H. Yu, K. Liang, M. Wang, Q. Wang, B. Yin and H. Chen, Reshaping the Tumor Immune Microenvironment Based on a Light-Activated Nanoplatform for Efficient Cancer Therapy, *Adv. Mater.*, 2022, **34**, e2108908.
12 W. Song, H. Yang, Y. Wang, S. Chen, W. Zhong, Q. Wang, W. Ding, G. Xu, C. Meng, Y. Liang, Z.-S. Chen, S. Cao, L. Wei and F. Li, Glutathione-Sensitive Photosensitizer-Drug Conjugates Target the Mitochondria to Overcome Multi-Drug Resistance in Cancer, *Adv. Sci.*, 2024, **11**, e2307765.
13 B. Q. Spring, I. Rizvi, N. Xu and T. Hasan, The role of photodynamic therapy in overcoming cancer drug resistance, *Photochem. Photobiol. Sci.*, 2015, **14**, 1476–1491.
14 R. Baskaran, J. Lee and S.-G. Yang, Clinical development of photodynamic agents and therapeutic applications, *Biomater. Res.*, 2018, **22**, 25.
15 M. R. Hamblin, Photodynamic Therapy for Cancer: What's Past is Prologue, *Photochem. Photobiol.*, 2020, **96**, 506–516.
16 T. Hu, Z. Wang, W. Shen, R. Liang, D. Yan and M. Wei, Recent advances in innovative strategies for enhanced cancer photodynamic therapy, *Theranostics*, 2021, **11**, 3278–3300.
17 G. Gunaydin, M. E. Gedik and S. Ayan, Photodynamic Therapy for the Treatment and Diagnosis of Cancer-A Review of the Current Clinical Status, *Front. Chem.*, 2021, **9**, 686303.
18 N. Alvarez and A. Sevilla, Current Advances in Photodynamic Therapy (PDT) and the Future Potential of PDT-Combinatorial Cancer Therapies, *Int. J. Mol. Sci.*, 2024, **25**, 1023.
19 M. Li, J. Xiong, Y. Zhang, L. Yu, L. Yue, C. Yoon, Y. Kim, Y. Zhou, X. Chen, Y. Xu, X. Peng and J. S. Kim, New guidelines and definitions for type I photodynamic therapy, *Chem. Soc. Rev.*, 2025, **54**, 7025–7057.
20 B. Lu, L. Wang, H. Tang and D. Cao, Recent advances in type I organic photosensitizers for efficient photodynamic therapy for overcoming tumor hypoxia, *J. Mater. Chem. B*, 2023, **11**, 4600–4618.
21 M. Li, Y. Xu, X. Peng and J. S. Kim, From Low to No O2-Dependent Hypoxia Photodynamic Therapy (hPDT): A New Perspective, *Acc. Chem. Res.*, 2022, **55**, 3253–3264.
22 M. Ju, L. Yang, G. Wang, F. Zong, Y. Shen, S. Wu, X. Tang and D. Yu, A type I and type II chemical biology toolbox to overcome the hypoxic tumour microenvironment for photodynamic therapy, *Biomater. Sci.*, 2024, **12**, 2831–2840.
23 L. Yu, Z. Liu, W. Xu, K. Jin, J. Liu, X. Zhu, Y. Zhang and Y. Wu, Towards overcoming obstacles of type II photodynamic therapy: Endogenous production of light, photosensitizer, and oxygen, *Acta Pharm. Sin. B*, 2024, **14**, 1111–1131.
24 Z. Zhou, J. Song, L. Nie and X. Chen, Reactive oxygen species generating systems meeting challenges of photodynamic cancer therapy, *Chem. Soc. Rev.*, 2016, **45**, 6597–6626.
25 Y.-Y. Zhao, L. Lu, H. Jeong, H. Kim, X. Li, H. Zhang and J. Yoon, Enhancing biosafety in photodynamic therapy: progress and perspectives, *Chem. Soc. Rev.*, 2025, **54**, 7749–7768.
26 D. Aebisher, S. Czech, K. Dynarowicz, M. Misiołek, K. Komosińska-Vassev, A. Kawczyk-Krupka and D. Bartusik-Aebisher, Photodynamic Therapy: Past, Current, and Future, *Int. J. Mol. Sci.*, 2024, **25**, 11325.
27 E. Gheybi, P. Hosseinzadeh, V. Tayebi-Khorrami, M. Rostami and M. Soukhtanloo, From reactive oxygen to cancer cell death: the science behind photodynamic therapy, *Laser Med. Sci.*, 2025, **40**, 448.
28 R. Kothari, N. K. Nambiar, V. Pundir, M. Chakravarty, D. Ramaiah, A. Nag and V. V. K. Venuganti, Localized delivery of Aza-BODIPY photosensitizer using dissolvable microneedle patch to treat oral carcinoma, *Int. J. Pharm.*, 2025, **681**, 125863.
29 N. Tyagi, R. K. K. Arya, D. Bisht, P. Wadhwa, T. Kumar Upadhyay, N. Kumar Sethiya, D. K. Jindal, S. Pandey and D. Kumar, Mechanism and potentialities of photothermal and photodynamic therapy of transition metal dichalcogenides (TMDCs) against cancer, *Luminescence*, 2024, **39**, e4770.
30 M. Tanaka, M. Kinoshita, Y. Yoshihara, N. Shinomiya, S. Seki, K. Nemoto, M. R. Hamblin and Y. Morimoto, Photodynamic therapy using intra-articular Photofrin for murine MRSA arthritis: biphasic light dose response for neutrophil-mediated antibacterial effect, *Laser Surg. Med.*, 2011, **43**, 221–229.
31 N. M. Bressler and S. B. Bressler, Photodynamic therapy with verteporfin (Visudyne): impact on ophthalmology and visual sciences, *Investig. Ophthalmol. Vis. Sci.*, 2000, **41**, 624–628.
32 J. F. Lovell, T. W. B. Liu, J. Chen and G. Zheng, Activatable photosensitizers for imaging and therapy, *Chem. Rev.*, 2010, **110**, 2839–2857.
33 H. Li, Y. Feng, Q. Luo, Z. Li, X. Li, H. Gan, Z. Gu, Q. Gong and K. Luo, Stimuli-activatable nanomedicine meets cancer theranostics, *Theranostics*, 2023, **13**, 5386–5417.
34 M. Liu and C. Li, Recent Advances in Activatable Organic Photosensitizers for Specific Photodynamic Therapy, *ChemPlusChem*, 2020, **85**, 948–957.
35 N. W. Nkune and H. Abrahamse, The Combination of Active-Targeted Photodynamic Therapy and

Open Access Article. Published on 29 January 2026. Downloaded on 5/27/2026 1:04:59 AM. This article is licensed under a Creative Commons Attribution-NonCommercial 3.0 Unported Licence.

Photoactivated Chemotherapy for Enhanced Cancer Treatment, *J. Biophot.*, 2025, **18**, e70005.
36 E. Nestoros, A. Sharma, E. Kim, J. S. Kim and M. Vendrell, Smart molecular designs and applications of activatable organic photosensitizers, *Nat. Rev. Chem.*, 2025, **9**, 46–60.
37 Y. Cai, T. Chai, W. Nguyen, J. Liu, E. Xiao, X. Ran, Y. Ran, D. Du, W. Chen and X. Chen, Phototherapy in cancer treatment: strategies and challenges, *Signal Transduct. Targeted Ther.*, 2025, **10**, 115.
38 S. Ma, S. Shi, X. Hu, Y. Zhao, B. Yang, M. Liao, B. Lu and Q. Xu, From basic to clinical translation: advances and perspectives of photodynamic nanodrugs, *Front. Pharmacol*, 2025, **16**, 1606372.
39 L. Fang, Z. Chen, J. Dai, Y. Pan, Y. Tu, Q. Meng, Y. Diao, S. Yang, W. Guo, L. Li, J. Liu, H. Wen, K. Hua, L. Hang, J. Fang, X. Meng, P. Ma and G. Jiang, Recent Advances in Strategies to Enhance Photodynamic and Photothermal Therapy Performance of Single-Component Organic Phototherapeutic Agents, *Adv. Sci.*, 2025, **12**, e2409157.
40 W. Zhu, L. Huang, C. Wu, L. Liu and H. Li, Reviewing the evolutive ACQ-to-AIE transformation of photosensitizers for phototheranostics, *Luminescence*, 2024, **39**, e4655.
41 D. Udhayakumari, Mechanistic Innovations in Fluorescent Chemosensors for Detecting Toxic Ions: PET, ICT, ESIPT, FRET and AIE Approaches, *J. Fluoresc.*, 2025, **35**, 3799–3828.
42 X. Li, S. Kolemen, J. Yoon and E. U. Akkaya, Activatable Photosensitizers: Agents for Selective Photodynamic Therapy, *Adv. Funct. Mater.*, 2017, **27**, 1604053.
43 S. Zeng, Z. Guo, Y. Hao, Y. S. Kafuti, Z. Yang, Q. Yao, J. Wang, X. Peng and H. Li, Tumor-microenvironment-activatable organic phototheranostic agents for cancer therapy, *Coord. Chem. Rev.*, 2024, **509**, 215786.
44 C. Zhao, T. Du, B. Zhu, Z. He, H.-Y. Wang and Y. Liu, Activatable near-infrared organic photosensitizers for imaging-guided photodynamic therapy, *Coord. Chem. Rev.*, 2025, **544**, 216962.
45 N. Kwon, H. Weng, M. A. Rajora and G. Zheng, Activatable Photosensitizers: From Fundamental Principles to Advanced Designs, *Angew Chem. Int. Ed. Engl.*, 2025, **64**, e202423348.
46 E. Nestoros, A. Sharma, E. Kim, J. S. Kim and M. Vendrell, Smart molecular designs and applications of activatable organic photosensitizers, *Nat. Rev. Chem.*, 2025, **9**, 46–60.
47 Q. Yu, J. Li, Y. Yu, M. Yan, D. Xu and S. Yin, Biomarker-activatable photosensitizers with aggregation-induced emission characteristics for photodynamic therapy, *Coord. Chem. Rev.*, 2024, **518**, 216056.
48 X. Wang, J. Peng, C. Meng and F. Feng, Recent advances for enhanced photodynamic therapy: from new mechanisms to innovative strategies, *Chem. Sci.*, 2024, **15**, 12234–12257.
49 S. Wang, L. Gai, Y. Chen, X. Ji, H. Lu and Z. Guo, Mitochondria-targeted BODIPY dyes for small molecule recognition, bio-imaging and photodynamic therapy, *Chem. Soc. Rev.*, 2024, **53**, 3976–4019.
50 J. Ma, R. Sun, K. Xia, Q. Xia, Y. Liu and X. Zhang, Design and Application of Fluorescent Probes to Detect Cellular Physical Microenvironments, *Chem. Rev.*, 2024, **124**, 1738–1861.
51 N. Soleja and M. Mohsin, Exploring the landscape of FRET-based molecular sensors: Design strategies and recent advances in emerging applications, *Biotechnol. Adv.*, 2024, **77**, 108466.
52 C. Wang, S. Wang, Y. Wang, H. Wu, K. Bao, R. Sheng and X. Li, Microenvironment-triggered dual-activation of a photosensitizer- fluorophore conjugate for tumor specific imaging and photodynamic therapy, *Sci. Rep.*, 2020, **10**, 12127.
53 G. Zheng, J. Chen, K. Stefflova, M. Jarvi, H. Li and B. C. Wilson, Photodynamic molecular beacon as an activatable photosensitizer based on protease-controlled singlet oxygen quenching and activation, *Proc. Natl. Acad. Sci. U. S. A.*, 2007, **104**, 8989–8994.
54 A. Stallivieri, L. Colombeau, J. Devy, N. Etique, C. Chaintreuil, B. Myrzakhmetov, M. Achard, F. Baros, P. Arnoux, R. Vanderesse and C. Frochot, New photodynamic molecular beacons (PMB) as potential cancer-targeted agents in PDT, *Bioorg. Med. Chem.*, 2018, **26**, 688–702.
55 D. Liu, B. Chen, Y. Mo, Z. Wang, T. Qi, Q. Zhang and Y. Wang, Redox-Activated Porphyrin-Based Liposome Remote-Loaded with Indoleamine 2,3-Dioxygenase (IDO) Inhibitor for Synergistic Photoimmunotherapy through Induction of Immunogenic Cell Death and Blockage of IDO Pathway, *Nano Lett.*, 2019, **19**, 6964–6976.
56 W. Shi, D. K. P. Ng, S. Zhao and P. Lo, A Phthalocyanine-Based Glutathione-Activated Photosensitizer with a Ferrocenyl Boron Dipyrromethene Dark Quencher for Photodynamic Therapy, *ChemPhotoChem*, 2019, **3**, 1004–1013.
57 Q. Wang, L. Yu, R. C. H. Wong and P.-C. Lo, Construction of cathepsin B-responsive fluorescent probe and photosensitizer using a ferrocenyl boron dipyrromethene dark quencher, *Eur. J. Med. Chem.*, 2019, **179**, 828–836.
58 K.-X. Teng, L.-Y. Niu, Y.-F. Kang and Q.-Z. Yang, Rational design of a "dual lock-and-key" supramolecular photosensitizer based on aromatic nucleophilic substitution for specific and enhanced photodynamic therapy, *Chem. Sci.*, 2020, **11**, 9703–9711.
59 J.-J. Cao, M.-S. Zhang, X.-Q. Li, D.-C. Yang, G. Xu and J.-Y. Liu, A glutathione-responsive photosensitizer with fluorescence resonance energy transfer characteristics for imaging-guided targeting photodynamic therapy, *Eur. J. Med. Chem.*, 2020, **193**, 112203.
60 M. Wu, W. Wu, Y. Duan, X. Liu, M. Wang, C. U. Phan, G. Qi, G. Tang and B. Liu, HClO-Activated Fluorescence and Photosensitization from an AIE Nanoprobe for Image-Guided Bacterial Ablation in Phagocytes, *Adv. Mater.*, 2020, **32**, 2005222.
61 X. Guo, H. Jin and P.-C. Lo, Encapsulating an acid-activatable phthalocyanine–doxorubicin conjugate and the hypoxia-sensitive tirapazamine in polymeric micelles for multimodal cancer therapy, *Biomater. Sci.*, 2021, **9**, 4936–4951.

© 2026 The Author(s). Published by the Royal Society of Chemistry

Open Access Article. Published on 29 January 2026. Downloaded on 5/27/2026 1:04:59 AM. This article is licensed under a Creative Commons Attribution-NonCommercial 3.0 Unported Licence.

62 L. K. B. Tam, J. C. H. Chu, L. He, C. Yang, K.-C. Han, P. C. K. Cheung, D. K. P. Ng and P.-C. Lo, Enzyme-Responsive Double-Locked Photodynamic Molecular Beacon for Targeted Photodynamic Anticancer Therapy, *J. Am. Chem. Soc.*, 2023, **145**, 7361–7375.
63 K. Wu, J. Liu, X. Zhang, Z. Chao, Y. Fang, Y. Zhu, Y. Liu, X. Zhang, Q. Wang, H. Ju and Y. Liu, Bovine serum albumin framed activatable NIR AIE photosensitizer for targeted tumor therapy, *Biomaterials*, 2025, **315**, 122918.
64 J. E. Barker, J. D. Tibbetts, C. T. J. Ferguson, Y. Xie and R. K. O'Reilly, Substituted Maleimides: Self-Reportable Linkers and Tags in Bioconjugation, Materials Science, and Nanotechnology, *Angew Chem. Int. Ed. Engl.*, 2024, **63**, e202410550.
65 X. Meng, Y. Shen, H. Zhao, X. Lu, Z. Wang and Y. Zhao, Redox-manipulating nanocarriers for anticancer drug delivery: a systematic review, *NanoBiotechnology*, 2024, **22**, 587.
66 L. Lin, X. Song, X. Dong and B. Li, Nano-photosensitizers for enhanced photodynamic therapy, *Photodiagnosis Photodyn. Ther.*, 2021, **36**, 102597.
67 E. Ortega-Forte, A. Rovira, M. López-Corrales, A. Hernández-García, F. J. Ballester, E. Izquierdo-García, M. Jordà-Redondo, M. Bosch, S. Nonell, M. D. Santana, J. Ruiz, V. Marchán and G. Gasser, A near-infrared light-activatable Ru(ii)-coumarin photosensitizer active under hypoxic conditions, *Chem. Sci.*, 2023, **14**, 7170–7184.
68 R. Zhan, W. Zhou, H. Ma, M. Zou, M. Zhang, W. Zhang and J. Tian, "Dual lock-and-key" triggered and endoplasmic reticulum targeting nanophotosensitizers for activatable Type-I photodynamic and photothermal therapies, *Chem. Sci.*, 2025, **16**, 12947–12955.
69 H. Niu, J. Liu, H. M. O'Connor, T. Gunnlaugsson, T. D. James and H. Zhang, Photoinduced electron transfer (PeT) based fluorescent probes for cellular imaging and disease therapy, *Chem. Soc. Rev.*, 2023, **52**, 2322–2357.
70 T. Maki, K. Shimoda, S. Aslam, R. Kyogoku, Y. Matsushita and Y. Tanaka, Oxygen-Independent Activatable Photosensitizers Based on the Control of Intersystem Crossing with a Tetrad-BODIPY Scaffold, *J. Org. Chem.*, 2025, **90**, 14177–14185.
71 N. Meher, D. Barman, R. Parui and P. K. Iyer, Recent development of the fluorescence-based detection of volatile organic compounds: a mechanistic overview, *J. Mater. Chem. C*, 2022, **10**, 10224–10254.
72 D. Escudero, Revising Intramolecular Photoinduced Electron Transfer (PET) from First-Principles, *Acc. Chem. Res.*, 2016, **49**, 1816–1824.
73 R. Wang, K.-H. Kim, J. Yoo, X. Li, N. Kwon, Y.-H. Jeon, S. Shin, S. S. Han, D.-S. Lee and J. Yoon, A Nanostructured Phthalocyanine/Albumin Supramolecular Assembly for Fluorescence Turn-On Imaging and Photodynamic Immunotherapy, *ACS Nano*, 2022, **16**, 3045–3058.
74 H. He, P. Lo and D. K. P. Ng, A Glutathione-Activated Phthalocyanine-Based Photosensitizer for Photodynamic Therapy, *Chem.–Eur. J.*, 2014, **20**, 6241–6245.
75 I. S. Turan, F. P. Cakmak, D. C. Yildirim, R. Cetin-Atalay and E. U. Akkaya, Near-IR Absorbing BODIPY Derivatives as Glutathione-Activated Photosensitizers for Selective Photodynamic Action, *Chem.–Eur. J.*, 2014, **20**, 16088–16092.
76 W. Hu, M. Xie, H. Zhao, Y. Tang, S. Yao, T. He, C. Ye, Q. Wang, X. Lu, W. Huang and Q. Fan, Nitric oxide activatable photosensitizer accompanying extremely elevated two-photon absorption for efficient fluorescence imaging and photodynamic therapy, *Chem. Sci.*, 2018, **9**, 999–1005.
77 Z. Liu, F. Song, W. Shi, G. Gurzadyan, H. Yin, B. Song, R. Liang and X. Peng, Nitroreductase-Activatable Theranostic Molecules with High PDT Efficiency under Mild Hypoxia Based on a TADF Fluorescein Derivative, *ACS Appl. Mater. Interfaces*, 2019, **11**, 15426–15435.
78 J. Zheng, Y. Liu, F. Song, L. Jiao, Y. Wu and X. Peng, A nitroreductase-activatable near-infrared theranostic photosensitizer for photodynamic therapy under mild hypoxia, *Chem. Commun.*, 2020, **56**, 5819–5822.
79 Y.-H. Zhang, X. Li, L. Huang, H. S. Kim, J. An, M. Lan, Q.-Y. Cao and J. S. Kim, AIE based GSH activatable photosensitizer for imaging-guided photodynamic therapy, *Chem. Commun.*, 2020, **56**, 10317–10320.
80 Y. Zhang, R. Zhao, J. Liu, H. Kong, K. Zhang, Y.-N. Zhang, X. Kong, Q. Zhang and Y. Zhao, Hierarchical nano-to-molecular disassembly of boron dipyrromethene nanoparticles for enhanced tumor penetration and activatable photodynamic therapy, *Biomaterials*, 2021, **275**, 120945.
81 H. Zhang, J. Pan, T. Wang, Y. Lai, X. Liu, F. Chen, L. Xu, X. Qu, X. Hu and H. Yu, Sequentially Activatable Polypeptide Nanoparticles for Combinatory Photodynamic Chemotherapy of Breast Cancer, *ACS Appl. Mater. Interfaces*, 2022, **14**, 39787–39798.
82 J. Miao, Y. Huo, G. Yao, Y. Feng, J. Weng, W. Zhao and W. Guo, Heavy Atom-Free, Mitochondria-Targeted, and Activatable Photosensitizers for Photodynamic Therapy with Real-Time In-Situ Therapeutic Monitoring, *Angew. Chem., Int. Ed.*, 2022, **61**, e202201815.
83 W. Lang, L.-Z. Chen, Y. Chen and Q.-Y. Cao, A GSH-activated AIE-based polymer photosensitizer for killing cancer cells, *Talanta*, 2023, **258**, 124473.
84 V. Lioret, K. Renault, O. Maury and A. Romieu, Valkyrie Probes: A Novel Class of Enzyme-Activatable Photosensitizers based on Sulfur- and Seleno-Rosamines with Pyridinium Unit, *Chem.–Asian J.*, 2023, **18**, e202300756.
85 D. Liu, M. Liang, Y. Tao, H. Liu, Q. Liu, W. Bing, W. Li and J. Qi, Hypoxia-accelerating pyroptosis nanoinducers for promoting image-guided cancer immunotherapy, *Biomaterials*, 2024, **309**, 122610.
86 F. Han, S. A. Abbas Abedi, S. He, H. Zhang, S. Long, X. Zhou, S. Chanmungkalakul, H. Ma, W. Sun, X. Liu, J. Du, J. Fan and X. Peng, Aryl-Modified Pentamethyl Cyanine Dyes at the C2' Position: A Tunable Platform for Activatable Photosensitizers, *Adv. Sci.*, 2024, **11**, 2305761.

Open Access Article. Published on 29 January 2026. Downloaded on 5/27/2026 1:04:59 AM. This article is licensed under a Creative Commons Attribution-NonCommercial 3.0 Unported Licence.

87 J. T. F. Lau, P.-C. Lo, X.-J. Jiang, Q. Wang and D. K. P. Ng, A Dual Activatable Photosensitizer toward Targeted Photodynamic Therapy, *J. Med. Chem.*, 2014, **57**, 4088–4097.
88 S. Kwiatkowski, B. Knap, D. Przystupski, J. Saczko, E. Kędzierska, K. Knap-Czop, J. Kotlińska, O. Michel, K. Kotowski and J. Kulbacka, Photodynamic therapy - mechanisms, photosensitizers and combinations, *Biomed. Pharmacother.*, 2018, **106**, 1098–1107.
89 S. Wang, R. Tian, X. Zhang, G. Cheng, P. Yu, J. Chang and X. Chen, Beyond Photo: Xdynamic Therapies in Fighting Cancer, *Adv. Mater.*, 2021, **33**, e2007488.
90 M. Essid and E. U. Mughal, Push-pull heterocycles and beyond: recent developments in absorption, emission, and ICT properties, *RSC Adv.*, 2025, **15**, 37609–37644.
91 M. Essid and E. Ullah Mughal, Push–pull heterocycles and beyond: recent developments in absorption, emission, and ICT properties, *RSC Adv.*, 2025, **15**, 37609–37644.
92 H. Ohno, S. Sumitani, E. Sasaki, S. Yamada and K. Hanaoka, Recent advances in fluorogenic probes based on twisted intramolecular charge transfer (TICT) for live-cell imaging, *Chem. Commun.*, 2025, **61**, 12871–12884.
93 R. Zhou, G. Liu, S. Fu, H. Zheng, D. Li, J. Dai, J. Wei, B. Li, C. Wang and G. Lu, Labeling selectivity of lipid droplets fluorescent probes: Twisted intramolecular charge transfer (TICT) vs intramolecular charge transfer (ICT), *Biosens. Bioelectron.*, 2024, **264**, 116624.
94 Z. Yang, W. Xu, J. Wang, L. Liu, Y. Chu, Y. Wang, Y. Hu, T. Yi and J. Hua, Diketopyrrolopyrrole-based multifunctional ratiometric fluorescent probe and γ-glutamyltranspeptidase-triggered activatable photosensitizer for tumor therapy, *J. Mater. Chem. C*, 2020, **8**, 8183–8190.
95 F. Xu, H. Li, Q. Yao, H. Ge, J. Fan, W. Sun, J. Wang and X. Peng, Hypoxia-activated NIR photosensitizer anchoring in the mitochondria for photodynamic therapy, *Chem. Sci.*, 2019, **10**, 10586–10594.
96 S. Lu, X. Lei, H. Ren, S. Zheng, J. Qiang, Z. Zhang, Y. Chen, T. Wei, F. Wang and X. Chen, PEGylated Dimeric BODIPY Photosensitizers as Nanocarriers for Combined Chemotherapy and Cathepsin B-Activated Photodynamic Therapy in 3D Tumor Spheroids, *ACS Appl. Bio Mater.*, 2020, **3**, 3835–3845.
97 Z. Cheng, S. Benson, L. Mendive-Tapia, E. Nestoros, C. Lochenie, D. Seah, K. Y. Chang, Y. Feng and M. Vendrell, Enzyme-Activatable Near-Infrared Hemicyanines as Modular Scaffolds for in vivo Photodynamic Therapy, *Angew. Chem., Int. Ed.*, 2024, **63**, e202404587.
98 J. Li, T. Wang, F. Jiang, Z. Hong, X. Su, S. Li and S. Han, A fluorescence-activatable tumor-reporting probe for precise photodynamic therapy, *J. Mater. Chem. B*, 2021, **9**, 5829–5836.
99 F. Liu, D. Zhu, Y. Li, M. Kong, Y. Li, J. Luo and L. Kong, A multifunctional near-infrared fluorescent probe for in vitro and in vivo imaging of γ-glutamyltranspeptidase and photodynamic cancer therapy, *Sens. Actuators, B*, 2022, **363**, 131838.
100 T. Almammadov, Z. Elmazoglu, G. Atakan, D. Kepil, G. Aykent, S. Kolemen and G. Gunbas, Locked and Loaded: β-Galactosidase Activated Photodynamic Therapy Agent Enables Selective Imaging and Targeted Treatment of Glioblastoma Multiforme Cancer Cells, *ACS Appl. Bio Mater.*, 2022, **5**, 4284–4293.
101 Y. Zhang, M. Zhao, J. Miao, W. Gu, J. Zhu, B. Cheng, Q. Li and Q. Miao, Hemicyanine-Based Type I Photosensitizers for Antihypoxic Activatable Photodynamic Therapy, *ACS Mater. Lett.*, 2023, **5**, 3058–3067.
102 J. Zhang, Y. Zhang, H. Zhang, W. Zhai, X. Shi and C. Li, A hypoxia-activatable theranostic agent with intrinsic endoplasmic reticulum affinity and type-I photosensitivity, *J. Mater. Chem. B*, 2023, **11**, 4102–4110.
103 E. Y. Xue, F. Kang, Y. Zhou and D. K. P. Ng, Design and synthesis of a NAD(P)H:quinone oxidoreductase 1-activatable photosensitiser for controlled photodynamic therapy, *Chem. Commun.*, 2023, **59**, 7056–7059.
104 Z. Li, Q. Feng, J. Hou and J. Shen, NQO-1 activatable NIR photosensitizer for visualization and selective killing of breast cancer cells, *Bioorg. Chem.*, 2024, **143**, 107021.
105 C. Cao, J. Li, X. Zhang, X. Zhang, X. Gong and S. Wang, NQO1-activated multifunctional theranostic probe for imaging-guided mitochondria-targeted photodynamic therapy and boosting immunogenic cell death, *Talanta*, 2024, **272**, 125786.
106 P. Barretta, F. Ponte and G. Mazzone, Rational design by DFT calculations of new metal complexes for photodynamic therapy based on an H2O2-Responsive Ir(III) photosensitizer activatable in physiological environment, *J. Mol. Liq.*, 2024, **402**, 124761.
107 C. Zhao, W. Sun, X. Huang, Y. Liu and H.-Y. Wang, Alkaline Phosphatase Activated Near-Infrared Frequency Upconversion Photosensitizers for Tumor Photodynamic Therapy, *J. Med. Chem.*, 2024, **67**, 13383–13391.
108 Q. Zeng, X. Li, J. Li, M. Shi, Y. Yao, L. Guo, N. Zhi and T. Zhang, Totally Caged Type I Pro-Photosensitizer for Oxygen-Independent Synergistic Phototherapy of Hypoxic Tumors, *Adv. Sci.*, 2024, **11**, 2400462.
109 X. Tian, L. C. Murfin, L. Wu, S. E. Lewis and T. D. James, Fluorescent small organic probes for biosensing, *Chem. Sci.*, 2021, **12**, 3406–3426.
110 F. Hecht, M. Zocchi, E. T. Tuttle, N. P. Ward, B. Smith, Y. P. Kang, J. Cazarin, Z. G. Soares, M. E. Ozgurses, H. Zhao, C. Sheehan, F. Alimohammadi, L. D. Munger, D. Trivedi, G. Asantewaa, S. K. Blick-Nitko, J. J. Zoeller, Y. Chen, V. Vasiliou, B. M. Turner, A. Muir, J. L. Coloff, J. Munger, G. M. DeNicola and I. S. Harris, Catabolism of extracellular glutathione supplies amino acids to support tumor growth, *BioRxiv*, 2024, preprint, DOI: 10.1101/2024.10.10.617667.
111 H. Sun, L. Li, R. Guo, Z. Wang, Y. Guo, Z. Li and F. Song, Suppressing ACQ of molecular photosensitizers by distorting the conjugated-plane for enhanced tumor photodynamic therapy, *Chem. Sci.*, 2024, **15**, 940–952.
112 J. C. H. Chu, J. Xiong, C. T. T. Wong, S. Wang, D. Y. Tam, A. García-Fernández, R. Martínez-Máñez and D. K. P. Ng,

© 2026 The Author(s). Published by the Royal Society of Chemistry

Open Access Article. Published on 29 January 2026. Downloaded on 5/27/2026 1:04:59 AM. This article is licensed under a Creative Commons Attribution-NonCommercial 3.0 Unported Licence.

Detection and Elimination of Senescent Cells with a Self-Assembled Senescence-Associated β-Galactosidase-Activatable Nanophotosensitizer, *J. Med. Chem.*, 2024, **67**, 234–244.

113 X.-Q. Wang, Q. Lei, J.-Y. Zhu, W.-J. Wang, Q. Cheng, F. Gao, Y.-X. Sun and X.-Z. Zhang, Cucurbit[8]uril Regulated Activatable Supramolecular Photosensitizer for Targeted Cancer Imaging and Photodynamic Therapy, *ACS Appl. Mater. Interfaces*, 2016, **8**, 22892–22899.

114 K.-X. Teng, L.-Y. Niu, Y.-F. Kang and Q.-Z. Yang, Rational design of a "dual lock-and-key" supramolecular photosensitizer based on aromatic nucleophilic substitution for specific and enhanced photodynamic therapy, *Chem. Sci.*, 2020, **11**, 9703–9711.

115 Y. Yang, W. Zhu, L. Cheng, R. Cai, X. Yi, J. He, X. Pan, L. Yang, K. Yang, Z. Liu, W. Tan and M. Chen, Tumor microenvironment (TME)-activatable circular aptamer-PEG as an effective hierarchical-targeting molecular medicine for photodynamic therapy, *Biomaterials*, 2020, **246**, 119971.

116 R. Song, T. Li, J. Ye, F. Sun, B. Hou, M. Saeed, J. Gao, Y. Wang, Q. Zhu, Z. Xu and H. Yu, Acidity-Activatable Dynamic Nanoparticles Boosting Ferroptotic Cell Death for Immunotherapy of Cancer, *Adv. Mater.*, 2021, **33**, 2101155.

117 Q. Zeng, X. Li, S. Xie, D. Xing and T. Zhang, Specific disruption of glutathione-defense system with activatable single molecule-assembled nanoprodrug for boosted photodynamic/chemotherapy eradication of drug-resistant tumors, *Biomaterials*, 2022, **290**, 121867.

118 H. Zhang, J. Pan, T. Wang, Y. Lai, X. Liu, F. Chen, L. Xu, X. Qu, X. Hu and H. Yu, Sequentially Activatable Polypeptide Nanoparticles for Combinatory Photodynamic Chemotherapy of Breast Cancer, *ACS Appl. Mater. Interfaces*, 2022, **14**, 39787–39798.

119 B. Li, J. Tian, X. Xie, F. Zhang, C. Wu, Y. Shan, G. Qi, W. Song, Y. Ping and B. Liu, Overcoming ROS Resistance of Photodynamic Therapy with Self-Assembled Nano-Prodrugs for Efficient Triple-Negative Breast Cancer, *Adv. Funct. Mater.*, 2024, **34**, 2309524.

120 S. Chen, B. Li, Y. Yue, Z. Li, L. Qiao, G. Qi, Y. Ping and B. Liu, Smart Nanoassembly Enabling Activatable NIR Fluorescence and ROS Generation with Enhanced Tumor Penetration for Imaging-Guided Photodynamic Therapy, *Adv. Mater.*, 2024, **36**, 2404296.

121 B. Li, J. Tian, X. Xie, F. Zhang, C. Wu, Y. Shan, G. Qi, W. Song, Y. Ping and B. Liu, Overcoming ROS Resistance of Photodynamic Therapy with Self-Assembled Nano-Prodrugs for Efficient Triple-Negative Breast Cancer, *Adv. Funct. Mater.*, 2024, **34**, 2309524.

122 Y. Yu, H. Jia, Y. Liu, L. Zhang, G. Feng and B. Z. Tang, Recent Progress in Type I Aggregation-Induced Emission Photosensitizers for Photodynamic Therapy, *Molecules*, 2022, **28**, 332.

123 Y. Zhang, C. Qian, Y. Chen, W. He and Z. Guo, Phototherapy via Modulation of β-Amyloid in Combating Alzheimer's Disease, *Aggregate*, 2025, **6**, e70020.

124 S. Ning, M. Lyu, D. Zhu, J. W. Y. Lam, Q. Huang, T. Zhang and B. Z. Tang, Type-I AIE Photosensitizer Loaded Biomimetic System Boosting Cuproptosis to Inhibit Breast Cancer Metastasis and Rechallenge, *ACS Nano*, 2023, **17**, 10206–10217.

125 V. K. Gawade, R. W. Jadhav and S. V. Bhosale, AIE-Based & Organic Luminescent Materials: Nanoarchitectonics and Advanced Applications, *Chem.–Asian J.*, 2024, **19**, e202400682.

126 D. Barman, K. Narang, R. Parui, N. Zehra, M. N. Khatun, L. R. Adil and P. K. Iyer, Review on recent trends and prospects in π-conjugated luminescent aggregates for biomedical applications, *Aggregate*, 2022, **3**, e172.

127 N. L. C. Leung, N. Xie, W. Yuan, Y. Liu, Q. Wu, Q. Peng, Q. Miao, J. W. Y. Lam and B. Z. Tang, Restriction of intramolecular motions: the general mechanism behind aggregation-induced emission, *Chem.–Eur. J.*, 2014, **20**, 15349–15353.

128 L.-H. Xiong, L. Yang, J. Geng, B. Z. Tang and X. He, All-in-One Alkaline Phosphatase-Response Aggregation-Induced Emission Probe for Cancer Discriminative Imaging and Combinational Chemodynamic–Photodynamic Therapy, *ACS Nano*, 2024, **18**, 17837–17851.

129 Y. Yuan, C. Zhang, M. Gao, R. Zhang, B. Z. Tang and B. Liu, Specific Light-Up Bioprobe with Aggregation-Induced Emission and Activatable Photoactivity for the Targeted and Image-Guided Photodynamic Ablation of Cancer Cells, *Angew. Chem., Int. Ed.*, 2015, **54**, 1780–1786.

130 S. Ji, H. Gao, W. Mu, X. Ni, X. Yi, J. Shen, Q. Liu, P. Bao and D. Ding, Enzyme-instructed self-assembly leads to the activation of optical properties for selective fluorescence detection and photodynamic ablation of cancer cells, *J. Mater. Chem. B*, 2018, **6**, 2566–2573.

131 Y. Wang, X. Liu, W. Wu, D. Mao, B. Wang, G. Tang and B. Liu, Mesoporous Rod-Like Metal-Organic Framework with Optimal Tumor Targeting Properties for Enhanced Activatable Photodynamic Therapy, *Adv. Ther.*, 2020, **3**, 2000011.

132 Q. Wu, Y. Li, Y. Li, D. Wang and B. Z. Tang, Hydrogen peroxide-responsive AIE probe for imaging-guided organelle targeting and photodynamic cancer cell ablation, *Mater. Chem. Front.*, 2021, **5**, 3489–3496.

133 X. Li, W. Xu, Z. Yang, S. Li, X. Gu, T. Yuan, C. Li, Y. Wang and J. Hua, A lipid droplet-targeted multifunctional AIE-active fluorescent probe for hydrogen peroxide detection and imaging-guided photodynamic therapy, *Sens. Actuators, B*, 2023, **375**, 132892.

134 K. W. K. Lam, J. H. C. Chau, E. Y. Yu, F. Sun, J. W. Y. Lam, D. Ding, R. T. K. Kwok, J. Sun, X. He and B. Z. Tang, An Alkaline Phosphatase-Responsive Aggregation-Induced Emission Photosensitizer for Selective Imaging and Photodynamic Therapy of Cancer Cells, *ACS Nano*, 2023, **17**, 7145–7156.

135 J. Tian, B. Li, F. Zhang, Z. Yao, W. Song, Y. Tang, Y. Ping and B. Liu, Activatable Type I Photosensitizer with Quenched Photosensitization Pre and Post Photodynamic Therapy, *Angew. Chem., Int. Ed.*, 2023, **62**, e202307288.

Open Access Article. Published on 29 January 2026. Downloaded on 5/27/2026 1:04:59 AM. This article is licensed under a Creative Commons Attribution-NonCommercial 3.0 Unported Licence.

136 Y. Liu, X. Wang, B. Wang, Z. Lu, C. Wu, Z. He, L. Jiang, P. Wei and T. Yi, Constructing Activatable Photosensitizers Using Covalently Modified Mesoporous Silica, *Adv. Sci.*, 2025, **12**, e2406887.

137 T. J. Harrison, X. Chen, K. Yasoshima and D. Bauer, Phototoxicity-Medicinal Chemistry Strategies for Risk Mitigation in Drug Discovery, *J. Med. Chem.*, 2023, **66**, 9345–9362.

138 Y. Yang, S. Jiang, S. G. Stanciu, H. Peng, A. Wu and F. Yang, Photodynamic therapy with NIR-II probes: review on state-of-the-art tools and strategies, *Mater. Horiz.*, 2024, **11**, 5815–5842.

139 R. Zhang, D. Yang, P. Zang, F. He, S. Gai, Y. Kuang, G. Yang and P. Yang, Structure Engineered High Piezo-Photoelectronic Performance for Boosted Sono-Photodynamic Therapy, *Adv. Mater.*, 2024, **36**, e2308355.

140 F. Akhtar, L. Misba and A. U. Khan, The dual role of photodynamic therapy to treat cancer and microbial infection, *Drug Discov. Today*, 2024, **29**, 104099.

141 J. Sun, K. Du, J. Diao, X. Cai, F. Feng and S. Wang, GSH and H_2 O_2 Co-Activatable Mitochondria-Targeted Photodynamic Therapy under Normoxia and Hypoxia, *Angew. Chem.*, 2020, **132**, 12220–12226.

142 H. S. Kocak, Z. Kilcan, P. Zhang, T. Almammadov and S. Kolemen, Dual enzyme responsive resorufin-based type-I/II photosensitizer for selective treatment of neuroblastoma cells under hypoxia, *Sens. Actuators, B*, 2026, **449**, 139077.

143 X. Wei, C. Zhang, S. He, J. Huang, J. Huang, S. S. Liew, Z. Zeng and K. Pu, A Dual-Locked Activatable Phototheranostic Probe for Biomarker-Regulated Photodynamic and Photothermal Cancer Therapy, *Angew. Chem., Int. Ed.*, 2022, **61**, e202202966.

144 H. Ding, L. Su, Z. Xie, A. D. Castano, Y. Li, L. R. Perez, J. Chen, K. Luo, X. Tian and G. Battaglia, Morphological insights in oxidative sensitive nanocarrier pharmacokinetics, targeting, and photodynamic therapy, *J. Mater. Chem. B*, 2025, **13**, 3852–3863.

145 N. W. Nkune and H. Abrahamse, Possible integration of artificial intelligence with photodynamic therapy and diagnosis: A review, *J. Drug Deliv. Sci. Technol.*, 2024, **101**, 106210.

146 Y. Liu, W. Xu, X. Qin, J. Zheng, B. Zheng, L. Sun, W. Zuo, D. Liu, Z. Liu, Y. Mou, H. Wang, Q. Zhang, J. Chen, P. Zhang and D. Zhang, Intravesical delivery of mucoadhesive and tumor-selective-penetrating nanozymes for enhancing the PDT of bladder cancer, *NanoBiotechnology*, 2025, **23**, 554.

147 M. Korbelik, Photodynamic therapy as immunogenic cell stress agent, *Photodiagnosis Photodyn. Ther.*, 2024, **46**, 104144.

148 M. Zeng, C. Hu, T. Chen, T. Zhao and X. Dai, Advancements in Cell Membrane-Derived Biomimetic Nanotherapeutics for Breast Cancer, *Int. J. Nanomed.*, 2025, **20**, 6059–6083.

149 J. Liao, L. Gong, Q. Xu, J. Wang, Y. Yang, S. Zhang, J. Dong, K. Lin, Z. Liang, Y. Sun, Y. Mu, Z. Chen, Y. Lu, Q. Zhang and Z. Lin, Revolutionizing Neurocare: Biomimetic Nanodelivery Via Cell Membranes, *Adv. Mater.*, 2024, **36**, e2402445.

150 O. C. Ioachimescu and R. Shaker, Translational science and related disciplines, *J. Invest. Med.*, 2025, **73**, 3–26.

151 P. Szymaszek, M. Tyszka-Czochara and J. Ortyl, Application of Photoactive Compounds in Cancer Theranostics: Review on Recent Trends from Photoactive Chemistry to Artificial Intelligence, *Molecules*, 2024, **29**, 3164.

152 *Fluorescent Chemosensors*, ed. L. Wu, A. C. Sedgwick, X.-P. He and T. D. James, The Royal Society of Chemistry, 2023.

© 2026 The Author(s). Published by the Royal Society of Chemistry